Characterizing Mechanical Behaviour of Polyethylene Material Using Finite Element Method

by

Azadeh Ebrahimian Hosseinabadi

A thesis submitted in partial fulfillment of the requirements for the degree of

Master of Science

Department of Mechanical Engineering
University of Alberta

Abstract

Approaches for accurate prediction of ductile failure of polyethylene (PE) pipe have been developed. The main objective of this thesis is to characterize deformation and mechanical behaviour of PE material under different conditions which contribute to PE failure. For this purpose, two different loading conditions are considered. One is the mostly used compressive loading in plastic pipe industry, named squeeze-off process. The other is a transverse loading which is a part of a test method to characterize environment stress cracking (ESC) of PE.

In the first part of this thesis, squeeze-off of PE pipe is simulated using finite element modelling. Squeeze-off is a widely used industrial procedure to block or reduce fluid flow in PE pipes. A set of experimental testing data was used to tune and extract elastic-plastic and creep material properties of a finite element (FE) model which consists of a pipe specimen and a squeezing bar. Squeezing speeds of 0.01, 1, and 50mm/min that cover common speeds used in the pipe repair or maintenance were used to model the squeeze-off process. A material sensitivity analysis was performed to identify parameters in the constitutive equations for which change of values yields a sensitive response of the deformation behaviour of PE. This study shows that identifying these parameters improves agreement between experimental data and finite element simulation. The FE model was then used to determine stress and strain distribution in the pipe specimen during the squeezed-off process.

In the second part of this thesis, an indentation loading that is used to generate deep stretch in a PE plate is simulated using FE modelling. Development of the indentation loading is part of a project to design a new test method to shorten the time for crack initiation in PE during the exposure to an aggressive agent. This method is used to accelerate time for characterizing PE's environmental stress cracking resistance (ESCR). Two cylindrical indenters of 13 and 7mm in diameter were modeled to generate the deep stretch in the central part of a circular area of 15mm in diameter. Through the FE modelling, stress variation and distribution are established during the deep stretch, but without the exposure to the aggressive agent. Data from the experimental testing was used to tune and extract information to quantify material behaviour. Three types of material input data were considered, one purely based on elastic-plastic (EP) deformation, another including damage generation, and the third including creep deformation, all of which were to calibrate input stress-strain curve by regenerating the load-stroke curve obtained from the experimental testing. Comparison of input stress-strain curves for the three types of FE modelling reveals the stress drops due to damage and creep, and their differences caused by the indenter size and loading speed used for the testing. The three types of input stress-strain curves also led to establishment of a stress-strain relationship for PE when no stress drop is caused by damage or creep. The study suggests that the stress-strain curve is more sensitive to the loading speed using the 7mm indenter. The FE modelling also shows more frequent stress relaxation during the deep stretch using the 7mm indenter than the 13mm indenter. Therefore, the study concludes that the 13mm indenter is more effective than the 7mm indenter in transforming the crystalline phase to the amorphous phase through the deep stretch, and thus is expected to generate ESCR with less scattering.

Preface

This thesis is an original work by Azadeh Ebrahimian under the supervision of Prof. P.-Y. Ben Jar. The main body of this thesis is composed of one published conference paper and one paper being considered for publication in *Journal of Polymer Engineering and Science*.

Chapter 2 of this thesis is mainly based on one published conference paper in *Canadian Society of Mechanical Engineering (CSME) congress*: A. Ebrahimian and P.Y.B. Jar, Finite Element Simulation on Squeeze-off of Polyethylene Pipes, CSNE 2020, University of Prince Edward Island, Canada. I was responsible for the analysis and simulation work, as well as the manuscript composition. Dr. Jar was the supervisory author and assisted with editing the manuscript.

Chapter 3 is based on one paper for submission to *Journal of Polymer Engineering and Science*: A. Ebrahimian and P.Y.B. Jar, Mechanical testing and Finite Element Modelling of Deep Stretch of Polyethylene Plate under Indentation Loading. I was responsible analysis and simulation work, as well as the manuscript composition. Dr. Jar was responsible for the data collection in the experimental testing and supervisory author and assisted with editing the manuscript.

Acknowledgements

I would like to express my sincere gratitude to my supervisor and mentor, Professor P.-Y. Ben Jar for his support, encouragement and guidance throughout my graduate studies. Thanks for providing the invaluable advice, persistent help without which I would not have finished my studies so smoothly. It has been a great experience to conduct research under his guidance.

Many thanks go to Natural Sciences and Engineering Research Council of Canada (NSERC) and Imperial Oil, the University Research Awards program for the financial support.

Lastly, and most importantly, I would like to thank my family for their unconditional love, presence and support, especially my dear parents and my beloved husband, Ehsan. You have always been my great source of power and support, without which I could not overcome difficulties during the course of this research.

Table of Contents

List of Tables

List of Figures

List of Symbols and Abbreviations

a, b, c, d, e, α, k, N, M, β, A,αk	Constants for constitutive model
CDM	Continuum damage mechanics
D	Overall damage variable/parameter
d	Damage variable
Dc	Critical damage value
E	Young modules
EP	Elastic-plastic
ESC	Environmental stress cracking
ESCR	Environmental stress cracking resistance
FEA	Finite element analysis
FEM	Finite element modelling
HDPE	high-density polyethylene
L	Minimum distance between the squeeze-off bars
k_s	Material parameter
PE	Polyethylene
p	Pressure
q	Von Mises stress
RP	Reference point
SCG	Slow crack growth
SCR	Slow crack resistant
t	Uncompressed pipe all thickness
$\bar{u}^{pl}$	Plastic displacement

$\bar{u}_f^{pl}$	Effective plastic displacement at the point of failure
WC	Wall compression
ε_n	Critical strain for the on-set of necking
ε_t	Strain at the beginning of the exponential hardening
ε_y	Transitional strain from linear to nonlinear deformation
$\dot{\bar{\varepsilon}}^{cr}$	Equivalent creep strain rate
$\dot{\bar{\varepsilon}}^{pl}$	Plastic strain rate
$\bar{\varepsilon}_S^{pl}$	Equivalent plastic strain at the onset of damage
θ_s	Shear stress ratio
λ	Stretch ratio
υ	Poisson's ratio
$\bar{\sigma}$	Effective stress in undamaged configuration
σ_{max}	Maximum normal stress
σ_{min}	Minimum normal stress
τ_{max}	Maximum shear stress

Chapter 1

1. Introduction

1.1. Background and motivation

Semi-crystalline polymers constitute a separate class of nanostructured materials. They are increasingly used in a wide range of applications such as pressure tubing, drainage and pipeline systems. Polyethylene (PE) as a type of semi-crystalline polymer is also known to have an excellent combination of strength, stiffness and dimensional stability for industrial applications. Nowadays, one of the main usages of PE is in the fabrication of low-pressure natural gas pipes with a life expectancy of 50 years. According to the most recent reports provided by U.S. Department of Transportation [1], PE is widely used to replace steel, concrete and clay as pipe material for natural gas transportation due to its durability, reliability, relative low cost, and ease for construction and maintenance. Moreover, statistics shows that almost 90% of the recently installed low-pressure gas pipeline systems are made of PE [2]. However, some inspection reports indicate the sudden failure of PE pipeline systems in the last four decades [3–5]. Therefore, there must be some blind spots that should be considered for characterizing PE pipes to evaluate their performance after the installation.

Some internal pressure tests on full-sized pipes at several temperatures have been conducted to investigate the long-term performance, design stress and service lifetime of PE pipe based on standard extrapolation methods like EN ISO 9080 and ASTM D2837. In this type of tests, the output curves are usually in terms of hoop stress versus failure time in a logarithmic scale, so the design stress at a desired temperature and lifetime can be estimated. The above hoop stress curves show that based on the stress level on the corresponding hoop stress curve, three types of failure are being expected in the pressurized PE pipe: (I) ductile failure, (II) brittle failure and (III) degradation-controlled failure. The main issue for the above test methods is that using full- sized pipes requires a long duration (around 1.3 year) for the test to be completed. Therefore, some other test methods have been developed to decrease the test time, including fully-notched test (FNCT) [6], the Pennsylvania edge-notched test (PENT) [7] and cracked round bar (CRB) test [8], to measure the resistance to slow crack growth (SCG) in brittle failure region of PE pipe.

This thesis presents finite element (FE) studies that represent two experimental approaches related to the mechanical behaviour and failure of PE material. One approach is the squeeze-off process which is a common practice in industry to close or control gas flow in gas pipes in order to perform maintenance and repair of the pipeline systems. For this purpose, the first part of the thesis explains a numerical model which has been developed to mimic the squeeze-off process. The same procedure has been carried out in a recent experimental study. The other approach is concerned about a failure behaviour of PE material, commonly known as environmental stress cracking (ESC). This failure has played a dominant role in long-term load-carrying performance of PE. For this purpose, the second part of the thesis presents an FE study on the use of indentation loading. This is a part of an approach to design a test method that can shorten time for crack initiation under the exposure to an aggressive agent, which can be used to characterize PE's environmental stress cracking resistance (ESCR). The thesis is to develop finite element (FE) modelling for both loading scenarios to mimic the actual deformation behaviours observed in the experiments. Material models have been developed to investigate the PE mechanical properties and failure mechanisms. Outputs from the FE models have been tuned with the experimental results to adjust the material properties.

It is known that external loading scenarios such as squeeze-off process as shown in Figure *1-1*, can cause degradation of mechanical properties and reduction of the remaining lifetime of the pipe [9,10]. Squeeze-off is a common practice in industry to close or control gas flow in gas pipes in order to perform maintenance and repair of the pipeline systems. However, inspections after the post squeeze-off process indicate that such a process could cause deterioration of mechanical properties, leading to unexpected, catastrophic failures of PE pipe over the long service time [11]. A number of studies have been conducted to investigate the effect of damage introduced by the squeeze-off process on both short- and long-term performance of PE pipe [12,13]. Degradation of mechanical properties resulting from the squeeze-off process leads to formation of slow crack growth (SCG) that generates brittle fracture over a long period [14,15]. Resistance of PE pipe to SCG can be characterized using different kinds of test methods that use full-sized pipe sections [16], notched specimens [17,18] or notched-free specimen [19]. Control parameters for the squeeze-off process include squeezing speed, release rate, squeeze-off ratio (also known as pipe wall compression ratio), geometry of the squeeze-off tool, PE pipe dimensions, and temperature, just to name a few, which may contribute to the change in the mechanical properties for PE pipe. A previous work considered the influence of squeezing ratio, pipe diameter and squeeze-off tool geometry on the pipe performance [20], in which the likelihood of damaging PE pipe increases by increasing the wall compression (WC) to a level of more than 30%. The definition of WC is given in Equation (1.1). *Figure 1-1* depicts the tool used to apply the desired WC.

$$WC = \left(1 - \frac{L}{2t}\right) \times 100\% \tag{1.1}$$

where *L* and *t* are the minimum distance between the squeeze-off bars and the uncompressed pipe wall thickness, respectively.

Figure 1-1 Commercial squeeze-off tool for PE pipe [14]

Although it is recommended in ASTM F 1734 [21] that the maximum WC should not be more than 30%, damage can also happen with WC less than 30%, especially for low slow crack resistant (SCR) materials. Therefore, it is very important to understand the squeeze-off phenomenon. Additionally, the studies indicate different pipe-grades of PE have different performance in the squeeze-off process [22]. There has not been much attention paid to the influence of squeezing speed on the mechanical property degradation. It should be noted that although the maximum squeezing speed is specified in standards such as ASTM F1041 [23], no work has been reported about the effect of squeezing speed on the performance of PE pipe. For this purpose, a study has been developed to investigate the effect of squeezing speed in the viewpoint of experimental testing and FE modelling [24]. Different loading speeds have been tested to investigate the effect of loading rate on the material response. Also, a FE model was developed to mimic the experimental results. The first part of this thesis is describing the use of an FE model to regenerate the material behaviour in a set of experimental tests to mimic the squeeze-off process ref. [24]. Although a similar FE approach has been utilized before, this work intended to improve the match with the experimental observation using a material model sensitivity analysis. The same loading speeds have been considered in the FE simulations.

One of the known types of slow crack growth in PE is “environmental stress cracking” or ESC. This type of cracks happens usually on the PE surface in contact with surface-active wetting agents such as alcohols, soaps, surfactants, etc. The surface-active agents do not chemically attack the polymer. However, they may cause microscopical effect and generate brittle-appearing fractures. In the absence of the surface-active environment, these fractures would not occur in any reasonable period of time under the same stress conditions. It is generally believed that these cracks are initiated at microscopic imperfections and propagate through the crystalline regions of the polymer structure. The ability of a polymer to resist slow crack growth or environmental stress cracking is known as ESCR. Different polymers exhibit different degrees of ESCR. Most of the current standards for characterizing ESCR require the use of a pre-notch to accelerate crack growth during the exposure to an aggressive agent (such as 10% Igepal CO-630 solution) [25,26]. These test methods use time for crack growth (during the exposure to an aggressive agent) to characterize

ESCR. However, variation of the pre-notch quality has been suspected to cause inconsistency of the test results. Another test method has been developed using notch-free specimens subjected to tensile stress in an aggressive environment. This test method uses strain hardening modulus to characterize resistance to ESCR [27,28]. However, results from the above tests are mainly used for prediction of the overall SCG resistance, not for determining the critical stress level for the SCG initiation. Since time for SCG initiation (t_{ini}) can account for 20%-80% of total time to failure (t_{tot}), it plays an important role for the reliability of PE pipe in the long-term service [29]. In view of the lack of test method to characterize resistance to SCG initiation, a new test method is being developed to use notch-free specimens to characterize ESCR. The new test method follows the same concept explained above that uses the post-yield strain hardening to indicate ESCR. The new test method consists of two stages. The first stage is to apply transverse loading to the center of a notch-free plate specimen to generate a truncated cone using an indenter. In the second stage, outer surface of the truncated cone is exposed to an aggressive agent to generate cracks in the highly stretched region. The main advantage with this method, comparing to the other methods above, is that indentation loading on a specimen used to determine t_{tot} and this test method can also be used to determine t_{ini} [30].

Computational models like FE are very effective in design of full-scale test components for prediction of a complex stress-strain distribution in the model. Creep and continuum damage models (CDM) are also available in FE software in order to predict accurately the deformation response of materials. However, it is impossible to consider both creep and damage simultaneously in most commercial FE software like ABAQUS. Damage characterization methods were mostly used for metallic materials. The damage variable *D*, is initially used as a geometry-based parameter, defined as the ratio of damaged to total cross-sectional area. Then the mechanical property-based methods are proposed that measure the damage based on the degradation of mechanical properties such as elastic modulus and yield or flow stress. Degradation of elastic modulus is used more often than stresses to explain damage especially for metals [31-33]. The current simplified damage evolution methods are based on various assumptions like strain-equivalent or energy-equivalent changes which describe the degradation of material after the onset of damage. The nonlinear rate-dependent deformation behaviour caused by viscous properties needs to be characterized for semi-crystalline polymers such as PE [34]. The effect of viscosity can be considered using a creep model.

The second part of this thesis describes a FE model which was developed to regenerate the indentation stretch of PE plate as explained in ref. [30]. The experimental tests have been conducted to confirm feasibility of the new approach to investigate ESCR of PE. As a part of tests, a transverse loading is applied to a PE plate using an indenter. Three separate material properties were considered to characterize the PE. One model used elastic-plastic input material properties. Another one used elastic-plastic with damage input material properties. In this model, an exponential damage evolution method is used to describe D as a function of displacement. The other material input properties were elastic-plastic with creep. The effect of viscous properties is considered using a time-hardening creep model separately to consider different loading scenarios.

1.2. Research objectives and approach

Despite that some progress has been made in modelling the PE deformation under different conditions, there are still a lot to do for improvement. The overall objective of this thesis can be divided into two approaches.

In the first approach FE results of a phenomenological modelling is used to investigate the effect of squeeze-off on mechanical properties of PE. For this approach sensitivity of material parameters in the constitutive material equation is examined to achieve a good match between the FE results and the material response obtained from the experimental study. Due to a long duration used in some of the experiments, the effect of viscous behaviour is considered in the FE model.

In the second approach, with the experience from the FE modelling of the squeeze-off process, a FE model is developed to investigate large deformation of PE under deep stretch subjected to transverse indentation, in a wide range of strain distribution which involves strains for yielding to large deformation at different location of the model. In this approach separate models considered damage initiation and growth based on the CDM concept, as well as the effect of creep on material response.

1.3. Thesis Organization

This thesis provides a detailed description of the proposed models and their applications to characterize the mechanical behaviour of PE material under different conditions. One is under the squeeze-off process and the other under transverse loading by an indenter. This thesis is composed of four chapters as follows.

Chapter 1 describes the background of the presented research and highlights the motivation behind the current research, research objectives and the proposed methodologies. Finally, the thesis outline is provided.

Chapter 2 presents a study on the effects of squeeze-off process on mechanical properties of PE pipe. Three squeezing speeds are used to cover the possible scenarios that may be encountered during the pipe repair or maintenance. This study shows that there is an acceptable agreement between experimental data and finite element simulation

Chapter 3 presents a phenomenon-based approach for combining experimental testing and finite element (FE) simulation for the purpose of investigating deep stretch of PE plate under indentation loading. The experimental work was conducted before, and the work presented in this thesis is to build a FE model to mimic the experimental results. The FE simulations were developed with consideration of damage evolution and creep separately. Results from the FE simulation suggest that the proposed approach enables the FE model to simulate both large deformation and stress drop in the final stage of the test.

Chapter 4 provides conclusions and recommendation for the future work.

References

[1] U.S. Department of Transportation, 2017. PHMSA - Data & Statistics [WWW Document]. US Department of Transportation. URL http://phmsa.dot.gov/portal/site/PHMSA/menuitem.6f23687cf7b00b0f22e4c6962d9c8789/?vgnextoid=a872dfa122a1d110VgnVCM10 0 0 0 09ed07898RCRD&vgnextchannel=3430fb649a2dc110VgnVCM10 0 0 0 09ed07898RCRD&vgnextfmt=print (accessed 3.6.20)

[2] Kiass, N., Khelif, R., Boulanouar, L., and Chaoui, K., 2005, "Experimental Approach to Mechanical Property Variability through a High-Density Polyethylene Gas Pipe Wall," J. Appl. Polym. Sci., **97**(1), pp. 272–281.

[3] Shalaby, H. M., Riad, W. T., Alhazza, A. A., and Behbehani, M. H., 2006, "Failure Analysis of Fuel Supply Pipeline," Engineering Failure Analysis, **13**(5), pp. 789–796.

[4] Azevedo, C. R. F., 2007, "Failure Analysis of a Crude Oil Pipeline," Engineering Failure Analysis, **14**(6), pp. 978–994.

[5] Majid, Z. A., Mohsin, R., Yaacob, Z., and Hassan, Z., 2010, "Failure Analysis of Natural Gas Pipes," Engineering Failure Analysis, **17**(4), pp. 818–837.

[6] ISO 16770., 2004, "Plastics-Determination of Environmental Stress Cracking (ESC) on Polyethylene (PE) – Full Notch Creep Test (FNCT)."

[7] 2005, *ISO 16241, Notch Tensile Test to Measure the Resistance to Slow Crack Growth of Polyethylene Materials for Pipe and Fitting Products (PENT)*, International Organization for Standardization.

[8] Pinter, G., Haager, M., Balika, W., and Lang, R. W., 2007, "Cyclic Crack Growth Tests with CRB Specimens for the Evaluation of the Long-Term Performance of PE Pipe Grades," Polymer Testing, **26**(2), pp. 180–188.

[9] Krishnaswamy, R. K., 2005, "Analysis of Ductile and Brittle Failures from Creep Rupture Testing of High-Density Polyethylene (HDPE) Pipes," Polymer, **46**(25), pp. 11664–11672.

[10] Palermo, G., 2004, "Correlating Aldyl 'A' and Century PE Pipe Rate Process Method Projections with Actual Field Performance," *Plastics Pipes XII Conference. Milan, Italy*.

[11] Brown, N., and Crate, J. M., 2012, "Analysis of a Failure in a Polyethylene Gas Pipe Caused by Squeeze off Resulting in an Explosion," J Fail. Anal. and Preven., **12**(1), pp. 30–36.

[12] Eugen, A., Emilia, O.M., 2015. Determining the forces in the polyethylene pipes after squeezing them off with specific equipment.

[13] Harris, K.E., 2007. Squeeze-off& gel patch repair methods for polyethylene pipe in natural gas distribution lines.

[14] M.B. Barker, J. Bowman, M. Bevis, the performance and causes of failure of polyethylene pipes subjected to constant and fluctuating internal pressure loadings, J. Mater. Sci. 18 (1983) 1095–1118. <http://link.springer.com/article/10.07/BF00551979>.

[15] R.W. Lang, A. Stern, G. Doerner, Applicability and limitations of current lifetime prediction models for thermoplastics pipes under internal pressure, Die Angew. Makromol. Chem. 247 (1997) 131–145, http://dx.doi.org/10.002/apmc.052470109/abstract (_ 1997 Hüthig & Wepf Verlag, Zug).

[16] ISO 9080, Plastics Piping and Ducting Systems-Determination of the Long-Term Hydrostatic Strength of Thermoplastics Materials in Pipe Form by Extrpolation, International Organization for Standardization, 2012.

[17] ISO 16770, Plastics-Determination of Environmental Stress Cracking (ESC) on Polyethylene (PE) – Full Notch Creep Test (FNCT), International Organization

for Standardization, 2004.

[18] M. Fleissner, Experience with a full notch creep test in determining the stress crack performance of polyethylenes, Polym. Eng. Sci. 38 (1998) 330–340,

http://dx.doi.org/10.002/pen.10194/abstract (Copyright _ 1998 Society of Plastics Engineers).

[19] Y. Zhang, P.Y. Ben Jar, Phenomenological modelling of tensile fracture in PE pipe by considering damage evolution, Materials and Design, 77 (2015) 72-82. <https://www.sciencedirect.com/science/article/abs/pii/S026130691500179X >.

[20] Yayla, P., Bilgin, Y., 2007. Squeeze-offof polyethylene pressure pipes: experimental analysis. Polym. Test. 26, 132–141. doi: 10.1016/j.polymertesting.20 06.09.0 06.

[21] ASTM F 1734-19 Standard Practice for Qualification of a Combination of Squeeze Tool, Pipe, and Squeeze-Off Procedures to Avoid Long-Term Damage in Polyethylene (PE) Gas Pipe. ASTM International, West Conshohocken, PA, 201**9**.

[22] "PE Squeeze-Off Tools - Reed Manufacturing" [Online]. Available: https://www.reedmfgco.com/en/products/plastic-pipe-tools/pe-squeeze-off-tools/. [Accessed: 09-Feb-2017].

[23] ASTM F1041-20, Standard Guide for Squeeze-Off of Polyolefin Gas Pressure Pipe and Tubing, ASTM International, West Conshohocken, PA, 2020.

[24] Y. Zhang, P.-Y, Jar, “Effect of squeeze-off on mechanical properties of polyethylene pipes”. International Journal of Solids and Structures.J, vol. 135, pp. 61–73, November 2017.

[25] D. C. Wright, Environmental stress cracking of plastics. Smithers Rapra Technology Ltd., Shawbury, UK (1996).

[26] 2. E. J. Kramer, Environmental cracking of polymers, in “Developments in Polymer Fracture. Vol. 1. Andrews EH (ed), Applied Science, London, Chap. 3 (1979).

[27] Cheng, J. J., Polak, M. A., and Penlidis, A., 2008, “A Tensile Strain Hardening Test Indicator of Environmental Stress Cracking Resistance,” Journal of Macromolecular Science®, Part A: Pure and Applied Chemistry, **45**(8), pp. 599–611.

[28] Kurelec, L., Teeuwen, M., Schoffeleers, H., and Deblieck, R., 2005, “Strain Hardening Modulus as a Measure of Environmental Stress Crack Resistance of High-Density Polyethylene,” Polymer, **46**(17), pp. 6369–6379.

[29] Chudnovsky, A., Zhou, Z., Zhang, H., and Sehanobish, K., 2012, “Lifetime Assessment of Engineering Thermoplastics,” International Journal of Engineering Science, **59**, pp. 108–139.

[30] P.Y.B. Jar, A New Concept of using Transverse Loading to Characterize Environmental Stress Cracking Resistance (ESCR) of Polyethylene (PE), Res Dev Material Sci, 3(5), 2018. <https://crimsonpublishers.com/rdms/pdf/RDMS.000574.pdf>.

[31] Lemaitre, J., and Dufailly, J., 1987, “Damage Measurements,” Engineering Fracture Mechanics, **28**(5–6), pp. 643–661.

[32] Bonora, N., Gentile, D., Pirondi, A., and Newaz, G., 2005, “Ductile Damage Evolution under Triaxial State of Stress: Theory and Experiments,” International Journal of Plasticity, **21**(5), pp. 981–1007.

[33] Celentano, D. J., and Chaboche, J.-L., 2007, “Experimental and Numerical Characterization of Damage Evolution in Steels,” International Journal of Plasticity, **23**(10–11), pp. 1739–1762.

[34] Jar, P.-Y. B., 2014, “Effect of Tensile Loading History on Mechanical Properties for Polyethylene,” Polym Eng Sci, **55**(9), pp. 2002–2010.

Chapter 2

2. Finite Element Simulation on Squeeze-off of Polyethylene Pipe

Squeeze-off is a widely used industrial procedure to block or reduce fluid flow in polyethylene (PE) pipes. In this study, squeeze-off of PE pipe is simulated using finite element modelling. A set of experimental testing data was used to tune and extract an elastic-plastic and creep material properties of a model which consists of a pipe specimen and a squeezing bar. Squeezing speeds of 0.01, 1, and 50mm/min that cover common speeds used during the pipe repair or maintenance were used to model the squeeze-off process. A material sensitivity analysis was performed to identify parameters in the constitutive equations for which change of values yields sensitive response of the deformation behaviour of PE. This study shows that identifying these parameters improves agreement between experimental data and finite element simulation. The finite element model was then used to determine stress and strain distribution in the pipe specimen during the squeezed off process

2.1. Introduction

Employing polyethylene (PE) pipes for natural gas transportation has been significantly increased in recent years due to its desirable physical and mechanical properties and superior corrosion resistance. A large portion of the natural gas distribution lines are made of PE pipes. One main advantage of PE pipes over the metallic counterparts is that a relatively straightforward and quick procedure, known as squeeze-off process, can be utilized to shut off or reduce gas flow when the pipeline requires maintenance or repair. Such a procedure is used more than half million times every year. Therefore, it is very important to investigate the influence of parameters that may affect mechanical properties of PE pipe after being subjected to this procedure.

Some researchers have conducted experimental studies to investigate the effect of squeeze-off on the mechanical behaviour of PE pipe. A study showed that failure behaviour in the PE pipe after the squeeze-off process [1] involves two failure modes, brittle fracture and slow crack growth (SCG). Although the latter was known to start from defects or third part impingement, the former could be generated without the presence of any defect in the material. The squeeze-off increases compressive stress across the pipe wall thickness, which is believed to induce the SCG development. That study concludes that by controlling the squeeze and release rates, failure could be avoided. Another experimental study designed a squeeze-off tool that could be used in a proper keyhole for squeezing by a single operator [2]. For this purpose, equations were developed to predict the required squeeze-off forces under different conditions, such as temperature, tool dimensions, and squeeze-off rate. In studies of long-term performance of PF pipe, lifetime of PE materials was analyzed at their in-ground temperature and pressure based on external loading modes, including rock impingement and pipe bending as the primary load, and squeezing load as the secondary load [3,4]. The SCG was regarded as a long-term failure mode for PE pipe in service. For damage initiation, results from of pipe testing suggest that the main parameters that govern damage formation are pipe wall compression, squeeze tool size, pipe thickness, and pipe material [5]. Some studies [6,7] investigated PE pipes of different wall thickness and pipe diameters to understand the effect of pipe wall thickness on damage generated in the squeeze-off process.

Numerical studies were also conducted on squeeze-off of PE pipes. One of the studies investigated stress and strain distribution in high-density PE (HDPE) pipes when they are subjected a squeeze-off load [8]. Another study [9] used a numerical model to quantify the influence of squeeze-off on degradation of mechanical properties for PE pipe. This study considered three squeezing speeds of 0.01, 1 and 50mm/min to cover the full range of possible squeeze-off scenarios that may be encountered during pipe repair or maintenance. Key outcomes from the simulation are reproduced in *Figure 2-1.* Although the simulation results show a reasonable agreement with the experimental data, some discrepancy exists, especially for the load drop during the stress relaxation stage. Such discrepancy leads to concerns about accuracy of the simulation and conclusions drawn from the study, that is, decrease of squeeze-off speed has no effect on the extent of mechanical property degradation of PE pipe. This conclusion is contradictory to the common belief that decrease of the squeezing speed should reduce the extent of degradation of mechanical properties for PE pipe [9].

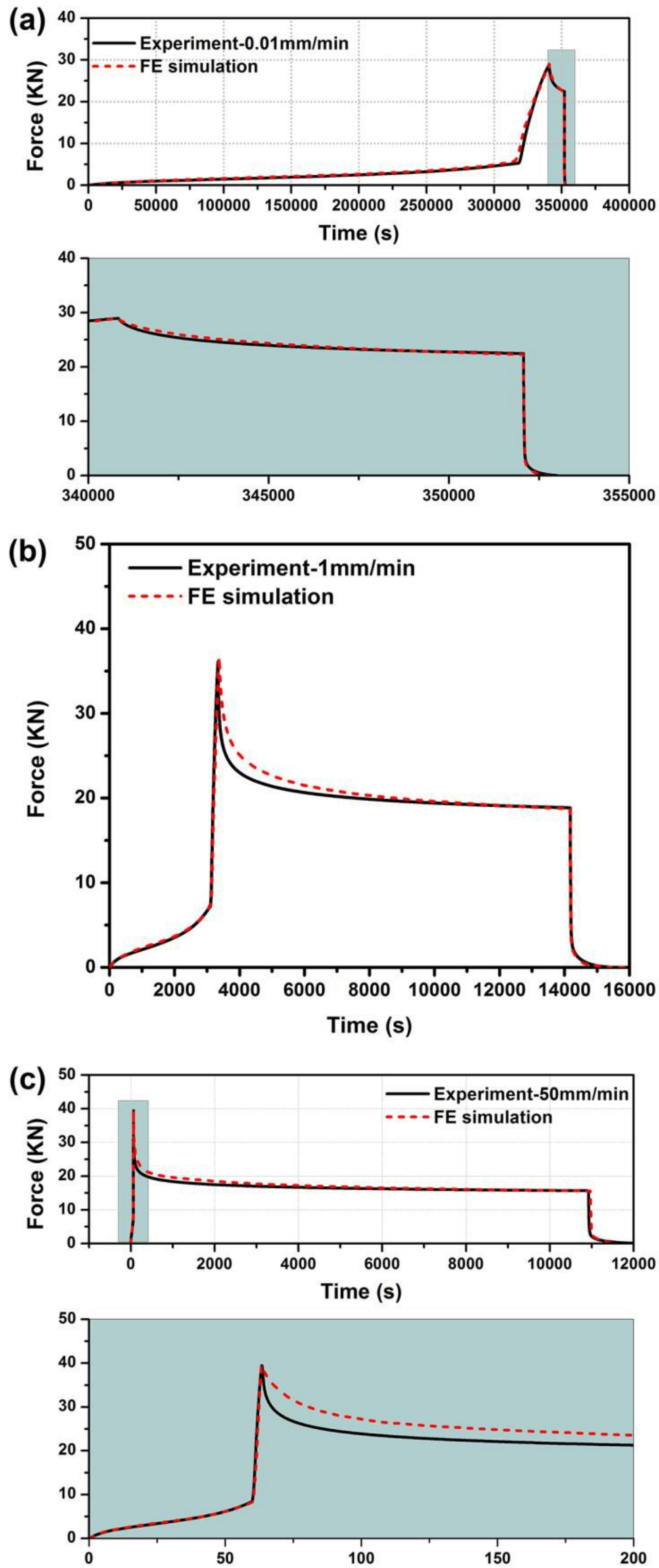

Figure 2-1 Comparison between FE simulation and experimental testing at squeezing speeds of 0.01 (a), 1 (b) and 50 mm/min (c) [9].

The squeeze-off process considered in the present work follows that used in ref. [9]. That is, the pipe samples were squeezed to the squeezing ratio of 30% at one of the crosshead speeds considered and kept at this squeezing ratio for 10,000 sec to mimic the maintenance procedure. Then the load was released at a constant crosshead speed of 0.1mm/min. *Figure 2-2* presents plots of force versus displacement for the three squeeze-off speeds considered in the previous study, in which points A to B is the first part of the squeezing process, till the inner pipe walls touch each other. The pipe is further squeezed until wall compression (WC) reaches 30%, which corresponds to point C in *Figure 2-2*. From points C to D, the squeezing tool is maintained at the same position for 10,000 seconds. Then, the squeezing bar is unloaded to point E [9].

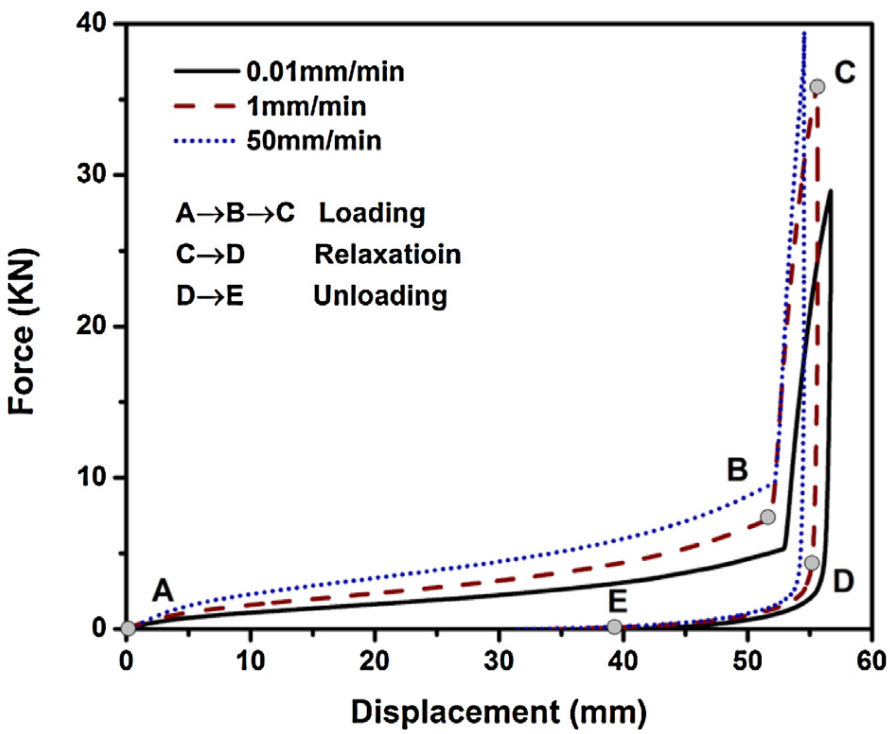

Figure 2-2 Variation of force with displacement at squeezing speeds of 0.01, 1, and 50 mm/min [9].

One of the challenges for quantifying the effect of squeeze-off speed on the PE pipe performance is the viscous behaviour of PE. In the previous work [9], performed in our research group, the squeeze-off process was simulated using finite element modelling (FEM), but the simulation results were not close enough to the experimental data, especially at squeeze-off speeds of 1 and 50mm/min.

Work presented in this paper is to examine possibility of reducing the difference between FEM simulation results and experimental measurements. For this purpose, the FEM simulation is based on the same experimental data as those used previously. The main difference between the current simulation approach and that used previously is that instead of the simple try-and-error approach, sensitivity of parameters used to prescribe material properties was first analyzed using a simple model under tensile loading. Parameters that showed strong influence on the load-time profile were identified and then used to tune the output from the squeeze-off model in order to reproduce the experimental results.

2.1. Finite element simulation

FEM was performed using ABAQUS to establish complex strain distribution generated in the PE pipe during the squeeze-off process. As mentioned in the previous section, in addition to the model for the squeeze-off process, a simple cylindrical model with constant cross section, under tensile loading, was performed to evaluate sensitivity of deformation to material parameters used to establish the stress-strain relationship for FEM of the squeeze-off process.

2.1.1. Squeeze-off Process

Geometry and Mesh Assignment

The model includes three parts, a PE pipe specimen, a squeeze-off bar and a rigid plane, as shown in *Figure 2-3*. Due to the geometric symmetry, the model consists of only half of the pipe length and quarter of the cross section, and the squeeze-off bar and the rigid plane were constructed as a rigid body. The rigid plane was to avoid extrusion passing the plane of symmetry. The pipe model consists of 27,000 C3D8R elements which are 8-node linear brick elements with reduced integration. There are 10 elements in the wall thickness direction and 30 elements along the quarter of the circumference. Size of the elements was chosen to be small enough to ensure convergence of the simulation results, based on a common mesh sensitivity analysis.

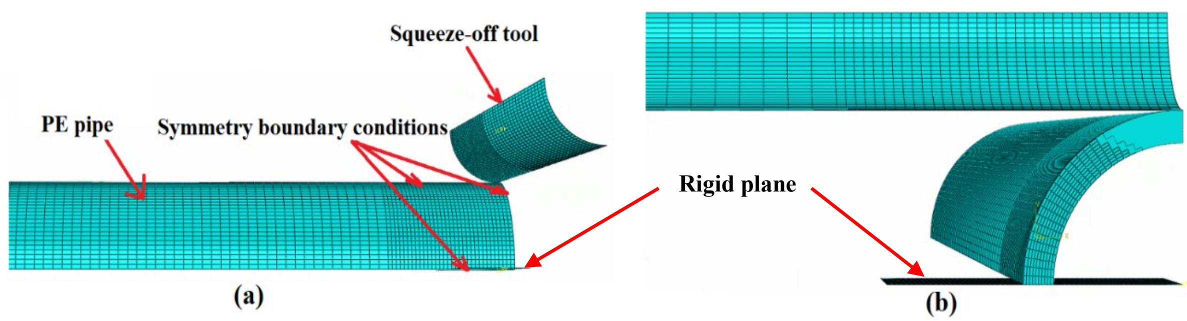

Figure 2-3 The front view (a) and side view (b) of a 3-D FE model for the squeeze-off process.

Solution Steps

Four steps were defined in the model to simulate the experimental tests. The 1st and 2nd steps were for the loading at a constant crosshead speed of 0.01, 1, or 50mm/min, till a squeezing ratio of 30% was reached. The 1st step introduced a significant portion of the loading and was purely based on the elastic-plastic behavior of the model, and the 2nd step involved a combination of elastic-plastic and creep deformation to take into account viscous behavior of the model. The 3rd step was for stress relaxation under constant displacement, which also included the elastic-plastic and creep deformation used in the 2nd step and lasted for 10,000 seconds. The 4th step was for unloading, again purely based on the elastic-plastic deformation.

Contact conditions

Two contact conditions have been defined in the model:

(i) Between the outer surface of the PE pipe and the squeeze-off bar: This contact is considered to be a hard contact in the normal direction, and frictional contact in the tangential direction with a friction coefficient of 0.08, based on results from an experimental study [10].

(ii) Between the inner surface of the PE pipe and the rigid plane: This contact is defined to avoid extrusion over the plane of symmetry. This contact is considered to be a hard contact in the normal direction, and frictionless contact in the tangential direction to avoid relative displacement of the pipe parts on each side of the symmetry plane.

Loading and Boundary Conditions

Boundary conditions for the model (as shown in *Figure 2-3*) are as follows:

(i) Planes of symmetry were defined on x-y, y-z and x-z planes.

(ii) For the loading step, a total displacement in y-direction was assigned to the reference point of the loading bar. The bar moved at the desired speed to achieve a squeezing ratio of 30% at the end of the loading step. In the stress relaxation step, the loading bar was kept stationary without any additional displacement. Finally, in the unloading step the bar returned back to its initial position.

(iii) The rigid plane was fixed and without any displacement and rotation.

Establishment of Input Material Properties

The constitutive equations proposed by Kwon and Jar [11] and later extended by Muhammad and Jar [12] were used to simulate deformation introduced by the squeeze-off process. The constitutive equation is based on the classical J_2 flow theory, and as shown in Equation (2.1) below, is expressed through a set of stress-strain relationships. Equation (2.1) consists of four expressions in four different strain ranges that cover both elastic and plastic deformation.

$$\sigma(\varepsilon)=\begin{cases} \dfrac{3}{2(1+\upsilon)}E\varepsilon & \varepsilon \le \varepsilon_y \quad \text{(a)} \\ d\left\{\left[a\left(\varepsilon+b\right)\right]^{(c-1)}-\left[a\left(\varepsilon+b\right)\right]^{(-c)}\right\}+e & \varepsilon_y \le \varepsilon \le \varepsilon_n \quad \text{(b)} \\ \alpha k \varepsilon^{N} & \varepsilon_n \le \varepsilon \le \varepsilon_t \quad \text{(c)} \\ k\exp\left(M\varepsilon^{\beta}\right) & \varepsilon \ge \varepsilon_t \quad \text{(d)} \end{cases} \tag{2.1}$$

where σ and ε are equivalent stress and equivalent strain, respectively, ε_y the transitional strain from linear to nonlinear deformation, ε_n the critical strain for the on-set of necking, and ε_t the strain at the beginning of the exponential hardening. Expression of equivalent stress is based on the von Mises stress, Equation (2.2), which is a function of all stress components σ_{ij}. Likewise, the expression of equivalent strain is based on Equation (2.3) which is a function of all strain components ε_{ij}.

$$\sigma_{EQ} = \frac{1}{\sqrt{2}}\{[(\sigma_{11}-\sigma_{22})^2+(\sigma_{22}-\sigma_{33})^2+(\sigma_{33}-\sigma_{11})^2]+6({\sigma_{12}}^2+{\sigma_{23}}^2+{\sigma_{31}}^2)\}^{1/2} \tag{2.2}$$

$$\varepsilon_{EQ} = \{\frac{2}{9}[(\varepsilon_{11}-\varepsilon_{22})^2+(\varepsilon_{22}-\varepsilon_{33})^2+(\varepsilon_{33}-\varepsilon_{11})^2]+\frac{4}{8}({\varepsilon_{12}}^2+{\varepsilon_{23}}^2+{\varepsilon_{31}}^2)\}^{1/2} \tag{2.3}$$

The other parameters (a, b, c, d, e, α, k, N, M, and β) are user-defined variables for which the values were determined from an iterative process until the time function of the reaction force in the loading bar from the FEM simulation, matched that from the experimental testing. In addition to Equation (2.1), a simple power-law creep function, as described in Equation (2.2), was introduced to increase strain under the same loading level in order to reproduce the experimental measurements.

$$\dot{\varepsilon} \qquad \qquad {}^{m} \tag{2.4}$$

where $\dot{\varepsilon}$ is the equivalent creep strain rate, t time measured from the start of the necking, σ the equivalent stress, and A, m, and n the user-defined fitting parameters.

Stress used to determine the equivalent creep strain rate in Equation (2.3) has the same expression as that given in Equation (2.2).

2.1.2. Sensivity of FEM to Material Parameters

To identify the fitting parameters to which the model stress output is more sensitive, an axisymmetric cylinder model of constant cross section was developed, subjected to tensile displacement.

As explained earlier, there are totally 5 mathematical expressions to describe the stress-strain relationship. Four expressions in Equation (2.1) describe the elastic-plastic behavior, and the expression in Equation (2.2) describes the creep (time-dependent) behaviour.

Note that Equation (2.1-c), for the necking, covers a wide strain range from 0.02 to 0.3 that was introduced in the squeeze-off process. As to be explained later, this strain range was established through adjusting load-time profile obtained from the FE model to match the experimental results. Because necking has a high rate of stress increase with the increase of strain, these parameters are expected to have a strong influence on the deformation behaviour of the model. Therefore, these parameters were investigated for their influence on the output stress from the model. In addition, variables in Equation (2.2) (i.e. A, n, and m) were also included in the sensitivity analysis, as they have been reported to have a considerable influence on the output strain at a given stress level [12].

In total, five parameters, two from Equation (2.1-c) and three from Equation (2.2), were considered for their influence on the output stress from the FEM model. This part of the simulation was conducted using a simple cylindrical model with constant cross-sectional area. *Figure 2-4* depicts this model and boundary conditions. As shown in the figure, the model is fixed at the bottom and subjected to upward displacement at the top. One loading step was used in the same time period as that used for the squeeze-off model, with the input material properties similar to those used for the squeeze-off simulation. This model was used to analyze sensitivity of the measured output stress to variation of five chosen parameters in the material model. Parameters that showed dominant roles on the output results were fine tuned in squeeze-off model.

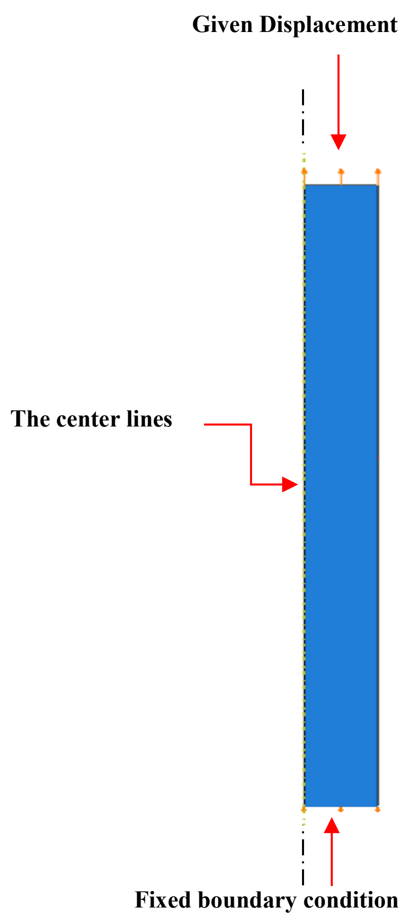

Figure 2-4 The simple tensile model and boundary conditions

The cylindrical model was first based on parameter values that were used in the previous study on the squeeze-off process [9]. Then, values for the five parameters, as mentioned above, were increased or decreased by 10%, one parameter each time while keeping values for the other four parameters unchanged. The corresponding output stress for the same element in the cylindrical model at the end of loading was recorded and compared to the output stress from the original model. Since the stress distribution was uniform in the model, each time an arbitrary element in the middle of the model was selected to record the stress output.

Information from the above study could reveal the parameters that showed the most influence on the output stresses, which were then the focus in the tuning process for the squeeze-off model in order to better fit the experimental measurements.

2.2. Results and discussion

Results are presented in the following order: sensitivity analysis, material and model development, and stress and strain contours.

2.2.1. Sensitivity Analysis in the Cylindrical Model

As mentioned before, sensitivity of the stress output to the value change for the five chosen parameters was analyzed to determine the most sensitive parameters. Table *2-1* shows results of the parameter sensitivity analysis. In both cases, results by either increasing or decreasing the parameter values by 10% suggest that parameter N in the exponential hardening equation and n in the creep equation caused a bigger difference in the output stress than the other parameters did with the same percentage change in the value. Therefore, these two parameters should be the most influential parameters for adjusting the output stress, and thus were tuned in the squeeze-off model in order to improve the closeness of the simulation results with the experimental measurements.

Other parameters in Equation (2.1- a to b) were changed based on the updated parameters in Equation (2.1-c) in order to establish a smooth stress-strain curve.

Table 2-1 Results from the parameters sensitivity analysis

	Increase of parameter values by 10%					**Decrease of parameter values by 10%**				
	A	n	m	αk	N	A	n	m	αk	N
Initial Value	$6.6E-20$	10	-0.61	18.1	0.07	$6.6E-20$	10	-0.61	18.1	0.07
New Value	$7.26E-20$	11	-0.67	19.9	0.77	$5.94E-20$	9	-0.55	16.33	0.063
Equivalent stress for the initial value (MPa)	17.227	17.2	17.227	17.227	17.227	17.227	17.227	17.227	17.227	17.227
Equivalent stress for the new value (MPa)	17.226	24.5	17.226	23.495	17.236	17.227	12.534	17.227	17.834	15.784
Stress change (%)	0.0058	42.5	0.0058	36.38	5.22	0.00	27.242	0.00	25.495	-8.37

2.2.2 Material and Model Development

As explained in section II, Finite Element Simulation, material parameters in Equation (2.1) were tuned in an iterative process to achieve a good agreement between the reaction force results from simulation and the experimental load-time data. *Table 2-2* lists the final values for parameters in Equation (2.1). *Figure 2-5* shows an example of the stress-strain curve obtained by replacing the parameters in the *Table 2-2* in the constitutive equation at the cross-head speed of 1mm/min.

Table 2-2 Values for parameters and strain range in Equations (2.1) and (2.2), determined from the FE simulation.

FE model			**Squeeze-off process**		
Crosshead speed (mm/min)			0.01	1	50
Equation (3a)		ε_y	0.05	0.005	0.005
		E	900	950	1100
		ν	0.4	0.4	0.4
Equation (3b)		ε_n	0.02	0.02	0.02
		a	20	20	29.5
		b	0.025	0.0354	0.018
		c	0.05	0.07	0.004
		d	-16.5	-50.3	-23.8
		e	14.3	15.5	20.62
Equation (3c)		ε_t	0.3	0.3	0.3
		αk	16.64	25.93	30.14
		N	0.07	0.07	0.07
Equation (3d)	Section 1	ε_{t1}	0.6	0.6	0.6
		K_1	14.3	22.281	26.35
		M_1	0.59	0.59	0.44
		β_1	1.8	1.8	1.8
	Section 2	ε_{t2}	0.8	0.8	0.8
		K_2	13.52	21.06	25.58
		M_2	0.71	0.71	0.5
		β_2	1.8	1.8	1.8
	Section 3	ε_{t3}	1.2	1.2	1.2
		K_3	11.43	17.924	23.55
		M_3	0.94	0.93	0.61
		β_3	1.8	1.8	1.8
	Section 4	ε_{t4}	2	2	2
		K_4	7.77	12.2	20.2
		M_4	1.2	1.2	0.71
		β_4	1.8	1.8	1.8
Equation (4)		$A \times 10^{15}$	6.6	6.6	9.6
		n	10	10	10
		m	-0.72	-0.96	-0.98

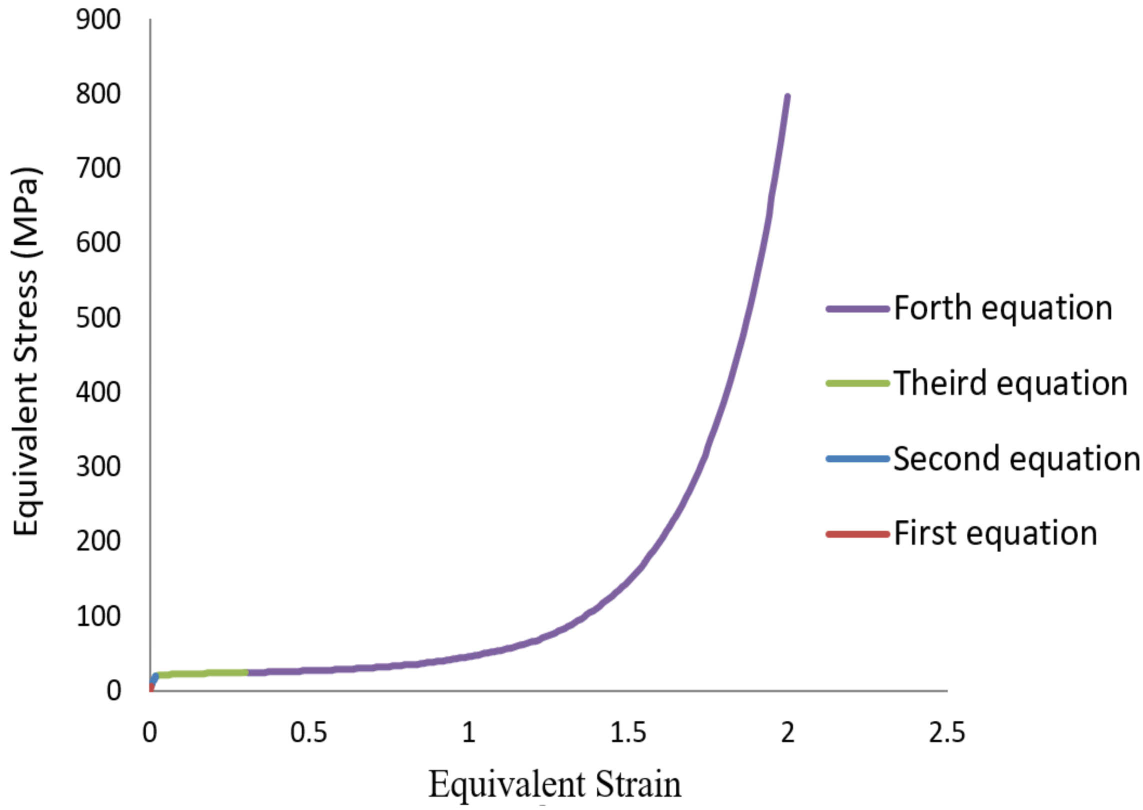

Figure 2-5 Equivalent stress-equivalent strain curves obtained by adjusting the parameters in the material behavior equation with the experimental data.

Figure 2-5 shows the equivalent stress-equivalent strain input curve in ABAQUS in which the elastic parameters (the Young's modulus and the Poisson's ratio), plastic material behavior (the relationship between yield stress and plastic strain) and time-hardening creep parameters are defined. After running the model, the relationship between reaction force and time in the squeezing bar was obtained from ABAQUS.

Figure 2-6 compares reaction force obtained from the FEM simulation with the experimental data at the same squeeze-off speeds. As shown in this figure, there is a good agreement between reaction force obtained from the FEM simulation and the experimental testing.

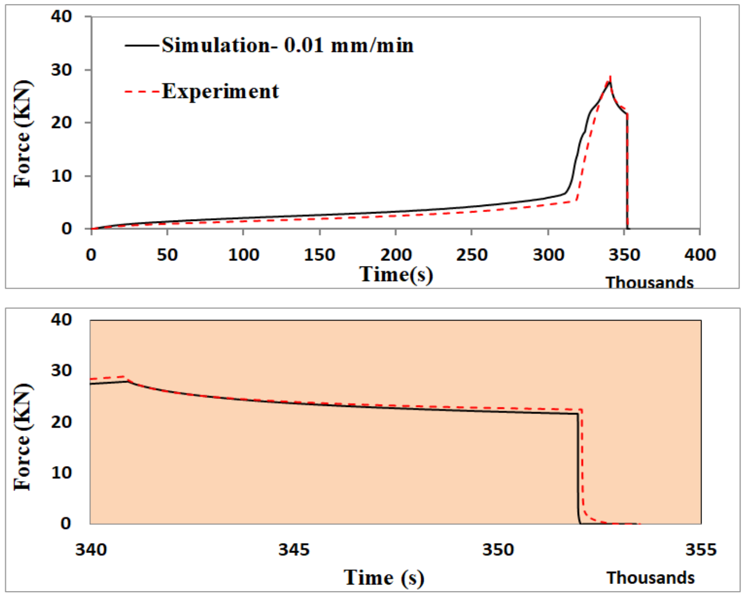

(a)

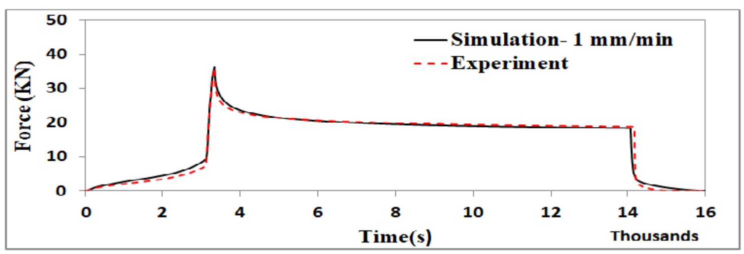

(b)

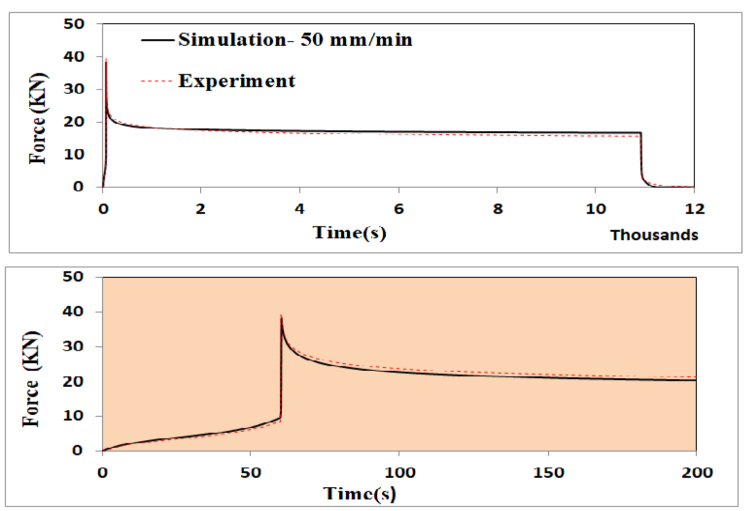

(c)

Figure 2-6 Comparison of FE simulation and experimental testing at squeezing speeds of 0.01(a), 1(b), and 50 mm/min (c).

2.2.2. Stress and Strain Development During Squeeze-off Process

As discussed earlier, squeeze-off process includes three main steps: loading, relaxation and unloading. *Figure 2-7* shows the equivalent stress contours in the specimen. *Figure 2-7(a)* was obtained at the beginning of the loading step, i.e. when the loading bar was first in contact with top pipe surface; *Figure 2-7(b)* was obtained at the beginning of the relaxation step, i.e. after the pipe wall has been compressed by 30%; *Figure 2-7(c)* was at the end of unloading step when the

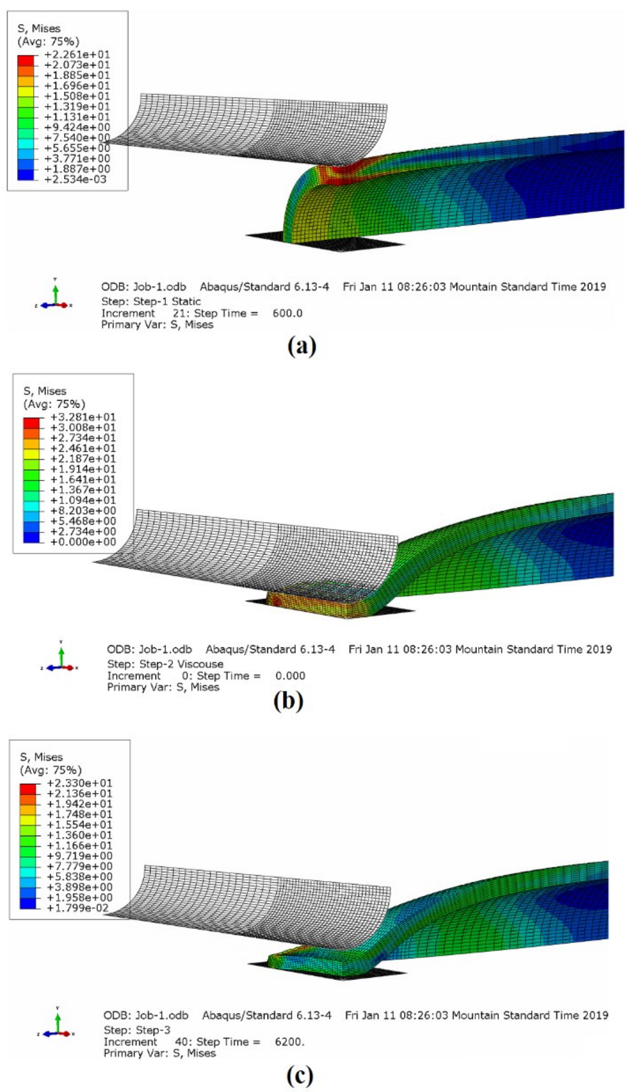

Figure 2-7 Equivalent stress contours (a) at the beginning of the loading step, (b) at the beginning of the relaxation steps, and (c) at the end of the unloading step.

loading bar was separated from the pipe. Note that due to plastic deformation introduced in the squeeze-off process, the bar did not return back to its initial position.

Summary and Conclusions

Work presented in this paper is to use a set of squeeze-off test results that were conducted in a previous study to explore the possibilities of determining the stress-strain relationship to improve the simulation accuracy. A three-dimensional finite element model was developed to mimic the squeeze-off process. This model includes a PE pipe specimen, squeeze-off bar and a rigid plane. Linear quadrilateral elements were assigned to the model parts. An elastic-plastic constitutive equation and a creep model were used to tune the model to match the experimental measurements. Furthermore, proper contacts, loads and boundary conditions were assigned to the model assembly to mimic the actual conditions in the squeeze-off process. Three steps were defined to load the model, including loading, relaxation and unloading steps. The results indicate that the constitutive equation can provide suitable stress-strain relationship to mimic closely the squeeze-off process. Moreover, the results suggest that due to plastic deformation, the pipe cannot return completely to its initial dimensions. As a result, significant degradation could be introduced by the squeeze-off process.

Acknowledgement

The work was sponsored by Natural Sciences and Engineering Research Council of Canada (NSERC), and Imperial Oil-the University Research Awards program.

References

[1] N. Brown and J.M. Crate, "Analysis of a Failure in a Polyethylene Gas Pipe Caused by Squeeze off Resulting in an Explosion," Fail. Anal. and Preven. J. Pennsylvania. USA, vol. 12, pp. 30–36, December 2011.

[2] K.E. Harris, "Squeeze-off& gel patch repair methods for polyethylene pipe in natural gas distribution lines", Corvallis.USA: Organ State University, 2007.

[3] G. Palermo, " Correlating Aldyl "A" and Century PE Pipe Rate Process Method Projections with Actual Field Performance", 2004, Milan. Italy.[Plastics Pipes XII Conference].

[4] D.R. Stephens, M.J. Cassady, B.N. Leis, "Progress report on preliminary screening tests on squeeze-off of polyethylene gas pipes", Battelle, Columbus, OH (United States), January 1987-December 1989.

[5] D.R. Stephens, B.N. Leis, R.B. Francini, M.J. Cassady, "Users' guide on squeeze-off of polyethylene gas pipes", vol.1, August 1989-February 1992. Battelle, Columbus, OH (United States).

[6] D.Uzelac, S. Bikiae, M. Durdeviae, I. Bordeasu, "Change of Polyethylene Pipe Wall Thickness after Squeezing Using Squeeze off-Tool", Materiale Plastice .J, vol.47, pp.461–466, December 2010.

[7] P. Yayla, Y. Bilgin, "Squeeze-off of polyethylene pressure pipes: Experimental analysis", Polymer Testing. J, vol. 26, pp.132–141, 2007.

[8] A. Egugen and O.M. Emilia, "Determining the Forces in the Polyethylen Pipes after Squeeezing Them off with Specific Equipments," AEECE, 2015 [International Conference on Advances in Energy, Environment and Chemical Engineering].

[9] Y. Zhang, P.-Y, Jar, "Effect of squeeze-off on mechanical properties of polyethylene pipes". International Journal of Solids and Structures.J, vol. 135, pp. 61–73, November 2017.

[10] S. Dhouibi, M. Boujelbene, M, Kharrat, M, Dammak, A, Maalej, "Friction Behavior of High-Density Polyethylene (HDPE) Against 304L Steel: An Experimental Investigation of the Effects of Sliding Direction, Sliding History and Sliding Speed", Journal of Surfaces and Interfaces of Materials.J, vol. 1, pp. 71–76, March 2013.

[11] H.J. Kwon, P.-Y. Jar, P.-Y.B, "On the application of FEM to deformation of high-density polyethylene.", International Journal of Solids and Structures.J , vol. 45, pp. 3521–3543, June 2008.

[12] S. Muhammad, P.-Y.B. Jar" Determining stress–strain relationship for necking in polymers based on macro deformation behavior", Finite Elements in Analysis and Design.J, vol. 70–71, pp. 36–43, September 2013.

[13] P.-Y. Ben Jar, S. Muhammad, "Cavitation-induced rupture in high-density polyethylene copolymers", Polymer Engineering & Science. J vol. 52, pp. 1005–1014, November 2011.

Chapter 3

3. Mechanical testing and finite element modelling of deep stretch of polyethylene plate under indentation loading

This paper presents a study that uses indentation loading to generate deep stretch of polyethylene (PE). This is part of a project to design a new test method to shorten the time for crack initiation during the exposure to an aggressive agent in order to accelerate the pace for characterizing PE's environmental stress cracking resistance (ESCR). Two cylindrical indenters of 13 and 7mm in diameter were used to generate the deep stretch in the central part of a circular area of 15mm in diameter. The study uses finite element (FE) modelling to establish the stress variation and distribution during the deep stretch, but without the exposure to the aggressive agent. Three types of material input data were considered for the FE modelling, one purely based on elastic-plastic (EP) deformation, another including damage generation, and the third including creep deformation, all of which were to calibrate input stress-strain curve by regenerating the stress-stroke curve obtained from the experimental testing. Objective of this study is three-folded. The first is to examine the possibility of using FE results to reproduce the experimental data at the loading stage of the tests; the second is to establish the elastic-plastic constitutive equations and stress drops caused by damage or creep deformation; the third is to investigate the influence of indenter size and loading speed on the constitutive equation, and their influence on stress drops due to damage generation or creep deformation. Comparison of the input stress-strain curves for the three types of FE modelling reveals the stress drops due to damage and creep, and their differences caused by the indenter size and loading speed used for the testing. The three types of input stress-strain curves also led to establishment of a stress-strain relationship for PE when no stress drop is caused by damage or creep, which suggests that the established stress-strain curve is more sensitive to the loading speed using the 7mm indenter. The FE modelling also suggests that stress relaxation occurs more frequently during the deep stretch using the 7mm indenter than the 13mm indenter. Therefore, the study concludes that the 13mm indenter is more effective than the 7mm indenter in transforming the crystalline phase to the amorphous phase through the deep stretch, and the 13mm indenter provides more consistent characterization of ESCR for PE.

3.1. Introduction

Polyethylene (PE) has been increasingly used to replace steel, concrete and clay to make components in infrastructures because of its strong chemical resistance, mechanical strength, affordability and ease for construction and maintenance. One of the examples is PE pipe which covers around 90% of pipes used for natural gas distribution [1, 2]. Although PE has good mechanical properties, it can develop brittle failure over a long period [3-7] which leads a huge, irrecoverable financial loss and service disruption. Therefore, it is important to identify and understand the effects of various parameters that could contribute to brittle failure of PE. Furthermore, in view that such brittle fracture may take a long time to develop in service, it is desired to have short-term tests available to evaluate the influence of these parameters on the development of brittle failure.

One of the major brittle failure modes, commonly known as environmental stress cracking (ESC), has played a dominant role in long-term load-carrying performance of PE [8]. It is well known that when PE pipes are in an environment that contains soaps, wetting agents, oils, or detergents, cracking can be generated on pipe surface after a long period in the environment. At this stage it is not clear about the rate of crack generation in the aggressive environment, but ESC is different from the slow crack growth in that the former has cracks generated over a large area without any noticeable plastic deformation, while the latter occurs in a very localized region. As a result, ESC resistance (ESCR) is a very important property for PE in order to reduce the likelihood of PE failure during its service life. This type of failure has been characterized by measuring time for the crack development in an environment that contains aggressive agents [9, 10]. Most of the tests use pre-notched specimens to accelerate the crack growth. However, due to advancement in polymer synthesis, test time to develop the crack growth has increased drastically (sometimes more than 5,000 hours), which also causes a significant data scattering, and thus is not reliable for accurate evaluation of ESCR [11, 12]. Furthermore, all existing methods for ESCR measurement cannot be used to characterize the resistance to ESC initiation as specimens used for the measurement already contain an artificial notch. It should be noted that some of the current standard methods for ESCR characterization, such as ISO 22088-2 (Method A), do not require specimens with any pre-notch. ISO 22088-2 (Method A) is to generate ESC when the notch-free specimens are subjected to a constant tensile load in the presence of chemical agent, which can be applied to evaluation of ESC difference in different environments, or among materials. However, a tedious testing procedure is needed to determine the appropriate loading level for crack generation in 100 hours, which involves multiple tests on specimens subjected to different loading levels. Such a complex process to determine the appropriate loading level for crack initiation can be very time-consuming.

There are two short-term test methods for ESCR measurement which do not rely on any pre-notch to generate crack growth. One method measures post-yield strain hardening modulus and the other the creep rate. The former uses results from a simple tensile test, based on a general relationship between post-yield strain hardening modulus and ESCR, that is, bigger the strain hardening modulus, longer the time for ESC development [13]. Since the simple tensile test is a short-term test, the strain hardening modulus can be used as a fast way to characterize ESCR for pipe-grade PE [14]. However, this test cannot be applied to characterization of ESCR for a given PE in exposure to different environments. The other test method, based on creep rate, uses oriented specimens. The results show a good correlation between the creep rate and the slow crack growth rate, indicating a strong effect of creep at the crack tip on the slow crack growth rate of the material [15,16]. However, results from this test method are very sensitive to loading level and closeness of the loading level to yield strength of the material. Therefore, this method is not applicable to comparison of ESCR of PEs with different yield strength.

Several studies on FE modelling have been conducted in the past, including the use of creep damage functions available in the finite element software [17-19]. Material constants for the creep damage function are determined using a uniaxial creep test on notched specimens, to obtain the material properties that are related to the multiaxial stress state. FE models are also used to establish viscoelastic and viscoplastic properties of glassy polymer, to separate the total deformation rate into elastic and inelastic components [20]. Some approaches use continuum damage mechanics (CDM) models for degradation of the constitutive equations to mimic fracture behavior of PE under tensile loading. These CDM models include creep damage models, ductile damage models, and fatigue fracture models. One study developed a creep damage model with parallel flat micro-cracks to describe damage-induced anisotropy and difference in damage and creep properties between tension and compression [21]. Fatigue failure was also investigated using damage models. Finite element analysis and damage evolution were used to determine the number of cycles for crack initiation [22]. For ductile damage, a three-dimensional model was developed using CDM to predict the deformation and degradation of PE. The analysis at the microstructural level considers the interaction between the amorphous and crystalline phases [23].

The ductile damage under different loading conditions was investigated using notched pipe ring (NPR) specimens in experimental testing at three crosshead speeds [24]. Results from the experimental testing were used as a reference to calibrate FE models in order to regenerate the specimen deformation either with or without the damage evolution. The results showed that the model with the damage evolution can regenerate both large deformation and ductile fracture, while the model without the damage evolution can only regenerate the large deformation before the final stress drop [24].

In the studies reviewed above, constitutive equations that are input to the FE model are adjusted so that the experimental test results can be regenerated using the FE model. However, no FE model has been developed to investigate the complex stress and strain distribution in a notched-free PE specimen that is subjected to deep stretch under the transverse loading.

This chapter presents results from a phenomenological FE modelling approach, based on experimental testing, to consider large, time-dependent deformation and degradation of mechanical properties. The experimental testing is part of a new test method for ESCR characterization, which is based on a concept similar to an approach reported in literature [25], to use the post-yield strain hardening to indicate the difference of ESCR. However, rather than using tensile loading on dog-bone specimens to generate the sufficiently large deformation to disintegrate the crystalline phase, the new approach uses indentation loading to introduce large deformation. This new approach consists of two steps. The first step is to apply the indentation loading to the central part of a notch-free plate to generate a truncated cone. The second step is to expose outer surface of the truncated cone to an aggressive agent to generate cracks in the highly stretched region. The overall idea and feasibility of the new approach have been presented in ref. [26]. One issue for the new approach is effectiveness of the indentation loading for disintegrating the crystalline structure. Unlike tensile loading, transverse indentation is known to generate a complex stress distribution profile in the specimen [25]. Yielding is expected to start along the circumference of the area in contact with the indenter, which could result in a stress drop to allow recrystallization. Issue addressed in this chapter is to determine the indenter size to maximize the amount of amorphous phase that can be generated from the deep stretch, by avoiding the stress-drop-induced recrystallization process.

Work described in this chapter consists of two parts. The first part is to conduct experimental testing to collect load-displacement curves using two indenters of different sizes, one being close to the diameter of the area available for the indentation and the other less than half of the diameter of the area. The second part is to use the finite element (FE) modelling to determine the stress evolution and distribution in the deformation process. In the second part, three series of FE simulation are considered. The first series is based purely on elastic-plastic stress-strain relationship, the second series includes the consideration of creep deformation, and the third series, rather than creep, considers the damage evolution. Using FE simulation to regenerate results from the experimental testing, elastic-plastic constitutive equations and stress drop caused by creep deformation and damage evolution are established. All in all, work described in this chapter is to use indentation loading to introduce deformation, and FE modelling to determine the corresponding stress response to the deformation. With the success of using FE models to mimic deformation generated in the experimental testing, results from the FE modelling are then used to evaluate the influences of indenter size and loading speed on the constitutive equation and stress drops due to damage or creep. Stress evolution determined from the FE models is also used to indicate the likelihood of stress relaxation using the two indenters during the deep drawing process, to evaluate the influence of indenter size on the efficacy of transforming the crystalline phase to the amorphous counterpart. In view of the strong viscous behaviour in the PE deformation, three loading speeds are considered in the study, to cover the possible range of test speed for the new approach. Therefore, the study includes the influence of loading speed on the constitutive equation and the corresponding stress drop induced by damage evolution or creep deformation.

3.2. Experimental details

Indentation loading used in this study is based on a concept similar to that recommended in the standard shear test (i.e. ASTM D732-17 [27]) but with an indenter smaller that the size available for the indentation, as the purpose for the indentation loading is to introduce deformation, not shear fracture. In this study, a cylindrical indenter was used to introduce the transverse loading on the central region of a plate specimen. The specimen was fixed along the edge using 8 bolts. *Figure*

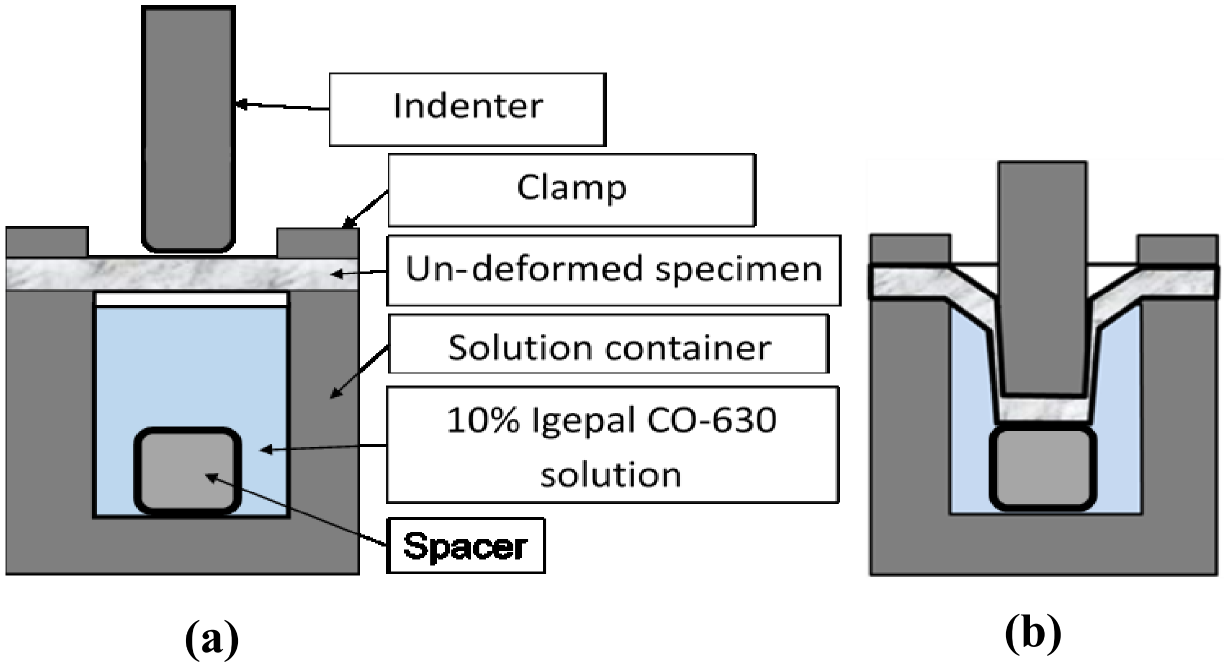

Figure 3-1 Schematic description of the new test approach: (a) the test set-up, and (b) indentation deformation that transforms the plate specimen in (a) to a truncated cone [25].

3-1(a) depicts the sectional view for the test set up, and *Figure 3-1(b)* the sectional view of a truncated cone introduced by the indenter.

Plaques of PE with octane co-monomer, provided by NOVA Chemicals, were used in the experiments. Number- and weight-average molecular weights, branch concentration (per 1000 C atoms), mass density, crystallinity, and tensile yield strength of the PE are listed in Table *3-1*. The PE plaques were compression-molded to rectangular shape of 3mm in nominal thickness and machined to square specimens of 40x40mm^2. For this study, two indenters of either 13 or 7mm in diameter were used. The solution container in *Figure 3.1(a)* has an inner diameter of 15*mm*, but in this study the container did not have any solution, simply used to introduce deformation constraint along the boundary. A plastic spacer is placed in the container to prevent the possibility of direct contact of the indenter with the container due to operation errors, as the contact could have damaged the indenter. Height of the truncated cone generated from the loading is around 5mm which is deemed to be a reasonable size for the ESC generation [26]. Three loading speeds of 1, 10 and 50mm/min were used to apply the indentation loading, using a home-made device installed in a Galbadini Quasar 100 universal test machine.

Table 3-1 Material characteristics of PE used in the study.

Material	M_n	M_w	Branches /1000 C	Density (g/cm^3)	Crystallinity [a] (wt%)	Tensile yield strength (MPa)
PE	30,391	73,074	3.4–4.2	0.941	63.6	20.2

[a] Calculated density (ρ) based on $X_c = \frac{\rho_c(\rho-\rho_a)}{\rho(\rho_c-\rho_a)}$, where X_c is crystallinity, ρ_c density of the crystalline phase (1.000 g/cm^3), and ρ_a density of the amorphous phase (0.853 g/cm3).

3.3. Finite element simulation

Finite element modelling (FEM) was performed using ABAQUS to determine the stress and strain distribution in the PE specimens, generated by the indentation loading. A two-dimensional, axisymmetric FE model was generated using ABAQUS/Standard (version 2019). The model consists of half of the sectional view of the test setup shown in *Figure 3.1(a)* and includes a PE specimen, an indenter to apply the load and a rigid substrate to mimic the deformation constraint introduced by the container as introduced in the experimental setup. *Figure 3-2 (a)* and *(b)* depict FE models for indenter size of 7 and 13mm, respectively.

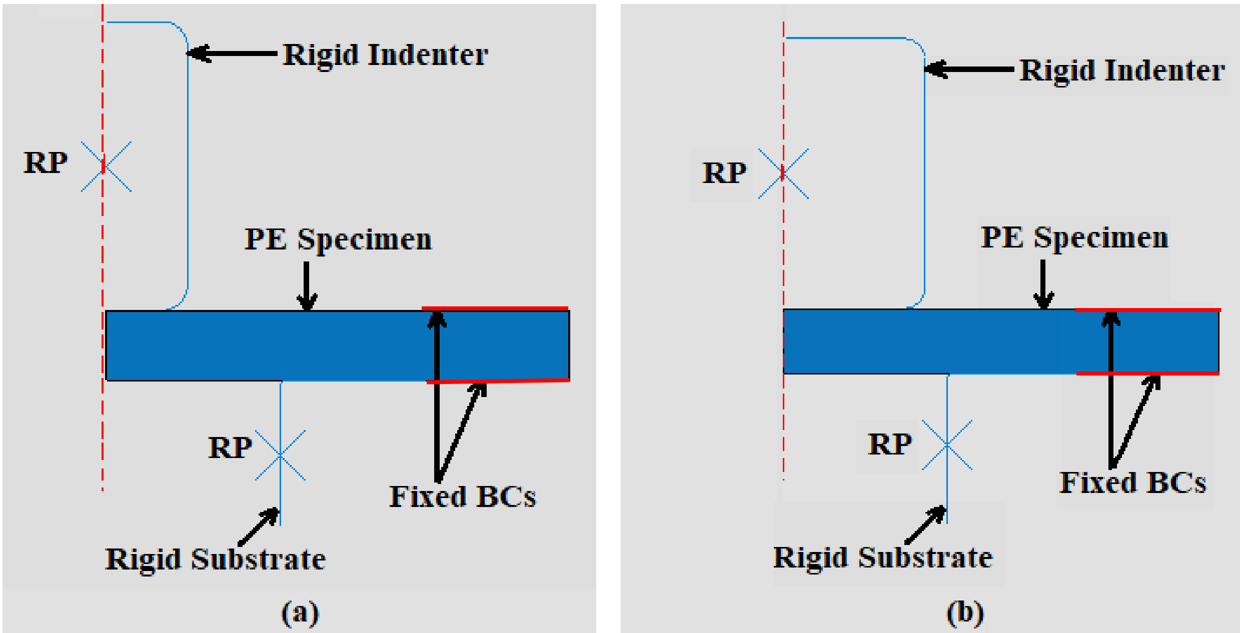

Figure 3-2 The axisymmetric FE model for the indentation tests: (a) for the indenter of 7mm in diameter, and (b) for the indenter of 13mm in diameter.

Dimensions of the FE models are the same as those used in the experimental testing. Each PE specimen in the FE models consists of 13415 CAX4 elements which are 4-node, bilinear, axisymmetric, quadrilateral elements of the first-order. Mesh sensitivity analysis has indicated that the element size is small enough to ensure convergence of the stress values. The indenter and substrate are modelled as analytical rigid bodies.

It should be noted that Abaqus does not allow simultaneous consideration of creep deformation and damage evolution. Therefore, three FE models were developed in order to consider creep deformation and damage evolution separately. The FE models use the built-in functions for damage and creep deformation provided in Abaqus. Then, by considering the difference of the output from these two models with the output from the phenomenological model without the consideration of creep or damage, to be named the base model, the influence of damage or creep on the stress drop can be determined. The phenomenological model is purely based on an elastic-plastic stress-strain input to capture the overall deformation behaviour for which the stress-strain input includes both creep deformation and damage evolution implicitly. The second model is named creep model which considers creep deformation using a power-law creep function as a separate input from the stress-strain input that has the damage evolution included in the stress-strain input. The third model is named damage model which rather than the creep deformation, considers damage evolution as a separate input from the stress-strain input which has the creep deformation included in the stress-strain input. All three models use a tabular form of input for the elastic-plastic stress-strain relationship which consists of approximately three thousand discrete points for a plastic strain range from 0 to 5.

Using the above three models, after the input material properties are calibrated for the models to mimic results from the experimental testing, stress drops caused by creep deformation and damage evolution can be established. That is, the stress drop by creep deformation can be determined by subtracting the stress-strain input for the base model from the corresponding input from the creep model, and likewise, the stress drop by damage evolution determined by subtracting the stress-strain input for the base model from the corresponding input for the damage model. Using this approach, influence of the indenter size and loading speed on the stress drop caused by creep deformation and damage evolution can be characterized. With these stress drops established, the equivalent stress-strain constitutive equation for deformation generated by the two indenters, without either creep or damage, can then be established and compared for deformation introduced by the two indenters.

Contact elements are used on the top surface of the specimen in *Figure 3.2* where the specimen is in contact with the indenter during the indentation loading. Friction at the contact is introduced with an adjustable friction coefficient in the range from 0.05 to 0.15 [28] which is adjusted based on the loading speed to smoothen the output curve of stress versus displacement so that it matches closely with the curve determined experimentally. A fixed boundary condition (BC) is applied between the specimen and the constraints, as shown in *Figure 3-2*, to limit both translation and rotation of the specimen at the boundary. Loading speed used in the experiment is introduced to the FE model by applying a time function of displacement at the reference point (RP) of the indenter in *Figure 3.2*. RP of the substrate, on the other hand, is fixed.

3.3.1. FE simulation using the base model

The first series of FE simulation adopted an elastic-plastic material model proposed in ref. [29-31], which is based on the classical J_2 flow theory without explicit expressions for damage or creep to simulate deformation introduced by the indenter. Equation (3.1) presents a series of expressions used to generate the stress-strain relationship used in different strain ranges of the deformation.

$$\sigma(\varepsilon)=\begin{cases} \dfrac{3}{2(1+\upsilon)}E\varepsilon & \varepsilon\le\varepsilon_y \quad \text{(a)} \\ d\left\{\left[a\left(\varepsilon+b\right)\right]^{(c-1)}-\left[a\left(\varepsilon+b\right)\right]^{(-c)}\right\}+e & \varepsilon_y\le\varepsilon\le\varepsilon_n \quad \text{(b)} \\ \alpha k\varepsilon^{N} & \varepsilon_n\le\varepsilon\le\varepsilon_t \quad \text{(c)} \\ k\exp\left(M\varepsilon^{\beta}\right) & \varepsilon\ge\varepsilon_t \quad \text{(d)} \end{cases} \tag{3.1}$$

where σ and ε are equivalent stress and equivalent strain, respectively, ε_y the transitional strain from linear to nonlinear deformation, ε_n the critical strain for the on-set of necking, and ε_t the strain at the beginning of the exponential hardening. The expressions for the equivalents stress and equivalent strain are the same as the expressions given in chapter 2, section 2.1.1. The other parameters (a, b, c, d, e, α, k, N, M, and β) are user-defined variables for which the values were determined from an iterative process until the stroke function of stress on the indenter from the FEM model, matched that measured from the experimental testing. Details of this iterative process are described in ref. [32].

It should be noted that although damage and creep were not considered explicitly, their effects have already been included in the parameter values in Equation (3.1).

3.3.2. FE simulation using the creep model

For this series of FE simulation, in addition to the expressions in Equation (3.1), a simple power-law creep function, as described in Equation (3.2), is used to increase strain at a given stress level with the increase of time after the equivalent strain reaches to the necking strain (ε_n) since PE has a strong viscous behaviour which results in the strain increase at a constant stress or the stress drop at a constant strain [33, 34].

$$\dot{\varepsilon}^{cr} = A\sigma^{n}t^{m} \tag{3.2}$$

where $\dot{\varepsilon}^{cr}$ is the equivalent creep strain rate, *t* time measured from the start of the necking, σ the equivalent stress, and *A*, *m*, and *n* the user-defined fitting parameters.

3.3.3. FE simulation using the damage model

For this series, damage evolution is explicitly expressed in addition to the elastic-plastic stress-strain relationship in Equation (3.1). Effect of damage is often reflected by a drop of the elastic modulus which could reduce the rate of stress increase during the loading phase.

In this study, damage evolution during the deformation process is characterized using damage variable *D*, defined in Equation (3.3) below based on the concept of continuum damage mechanics (CDM).

$$\sigma = (1 - D)\bar{\sigma} \tag{3.3}$$

where D is the damage variable and $\bar{\sigma}$ the effective (or undamaged) stress tensor. In general, material loses its load-carrying capability when D reaches a critical damage level (D_C), and the element can be removed from the FE model [35-37]. In this study, based on the suggestions given in ref. [38,39], damage was expected to start at the onset of necking, i.e. when the strain reaches ε_n at the loading stage. However, as to be shown later, a stress distribution profile generated by the indentation loading is highly non-uniform. Therefore, influence of damage on the model's load response to deformation was not noticeable until some elements have experienced strains in the range for the necking, Equation 3.1(c). In view of this problem, FE simulation conducted in this study introduced damage only when strain reaches the necking stage, i.e. $\varepsilon \geq \varepsilon_n$. The same approach is applied to the creep deformation, that is, creep deformation is introduced only in the necking stage, i.e. $\varepsilon \geq \varepsilon_n$. In addition, since no data are available for the damage-induced change of mechanical properties, the damage model used the damage evolution as part of the fitting variables. This included critical damage level and the damage evolution. The critical damage level, D_C, is assumed to have a value in the range from 0.8 to 1 which served as an adjusting parameter to fit the output from the damage model to the results from the experimental testing. Damage evolution is based on shear damage for which the adjustable variables are described below.

I) Criterion for the onset of damage: In this work, it is assumed that the equivalent plastic strain at the onset of damage ($\bar{\varepsilon}_S^{pl}$) is a function of shear stress ratio (θ_s) and plastic strain rate ($\dot{\bar{\varepsilon}}^{pl}$). The shear stress ratio is defined in Equation (3.4).

$$\theta_s = \frac{q + k_s p}{\tau_{max}} \tag{3.4}$$

with $$\tau_{max} = \frac{\sigma_{max} - \sigma_{min}}{2} \tag{3.5}$$

where q is the von Mises stress, p is pressure, τ_{max} the maximum shear stress of a given stress state, define in Equation (3.5) [40], and k_s a material parameter.

In the FE simulation, values of q, p and τ_{max} were determined from the output of the base model in an element of a highly stretched region. Since damage was considered to start at the onset of necking, q, p and τ_{max} at ε_n of the base model are used to calculate θ_s and $\dot{\bar{\varepsilon}}^{pl}$.

II) Damage evolution law: The damage evolution law adopted is to mimic the rate of material stiffness decrease once the damage is initiated. For this, an exponential function is used to describe the damage evolution, as shown in Equation (3.6).

$$d = \frac{1 - e^{-\alpha\left(\bar{u}^{pl}/\bar{u}_f^{pl}\right)}}{1 - e^{-\alpha}} \tag{3.6}$$

where d is the damage variable, $\bar{u}^{pl}$ the effective plastic displacement, $\bar{u}_f^{pl}$ the critical effective plastic displacement at which the element is eliminated from the model and α an adjustable exponent. It should be noted that the overall damage variable (D) captures the combined effect of individual damage variables (d_i) in the model of anisotropic materials such as fibre composites. Therefore, for the model developed in the current study d can be assumed to be equal to D [40]. FE simulation using the damage model is focused on the two main stress drops observed in the experiments. The first stress drop occurred at the onset of necking and the other stress drop at the final loading stage before the unloading when the deep drawing was generated using the 7mm indenter. All simulations were conducted based on the assumption that the exponent α could be adjusted so that results generated in the stress drop stage of the model is consistent with that

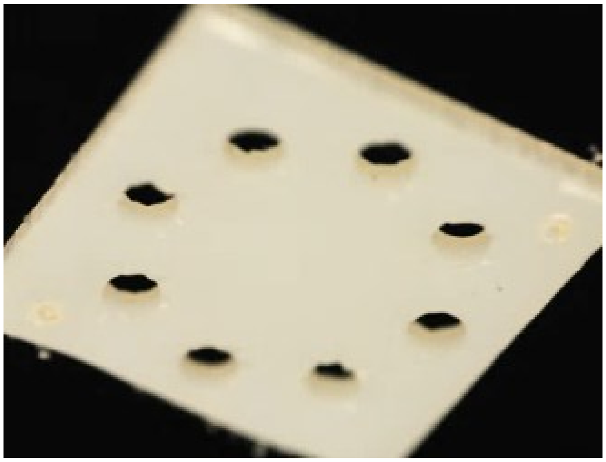

Figure 3-3 Typical plate specimens before the test (left) and after the test (right) using the 13mm indenter at the loading speed of 10mm/min.

observed from the experimental testing. The plastic displacement at the onset of failure $\left(\bar{u}_f^{pl}\right)$ was also considered as an adjustable parameter for the simulation of the damage evolution.

Totally, the additional adjusting variables for the damage model are $\alpha, \bar{u}^{pl}$ and D_C. An iterative process was used to determine values for these variables in order for the stress-stroke curve generated from the FE model to match with that obtained from the experiment.

3.4. Results and discussion

3.4.1 Test Results

Photographs for a typical specimen before and after the test using the 13mm indenter at the loading speed of 10mm/min are presented in *Figure 3-3*. The photograph on the right shows no visible cracks in the annular region of the truncated cone.

Figure 3-4 shows a schematic depiction of load versus logarithmic displacement that contains four stages. Stage 1 is for the initial contact between the indenter and the specimen, stage 2 for the stretch of the specimen before the yielding, stage 3 for the yielding which is gradually developed through the specimen thickness, and stage 4 for the deep drawing at which the truncated cone is generated.

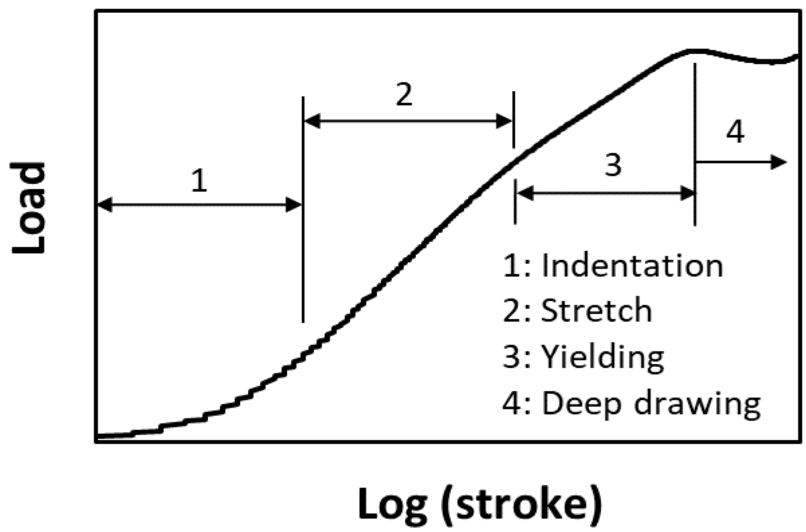

Figure 3-4 Schematic depiction of load-displacement curve from the loading stage of the test.

Stress is calculated by dividing the load by the product of specimen thickness and indenter circumference. *Figure 3-5* presents typical curves of engineering stress versus stroke generated from the indentation test using 7 and 13mm indenters for *(a)* and *(b)*, respectively. Stress is used rather than force in order to normalize the force due to variation in specimen thickness. For each indenter size, three loading speeds of 1, 10 and 50mm/min were used. The overall trend is similar to that reported in ref. [41], that is, within the loading speeds used in this study, both yield stress and the corresponding stroke increase with the increase of the loading speed. Curves in *Figure 3-5(b)*, using 13mm indenter, also show nearly a plateau region after the first stress drop, in the stroke range from 6 to 10mm. For the 7mm indenter, *Figure 3-5(a)*, the plateau region is much shorter, followed by a second stress drop before the end of the loading stage.

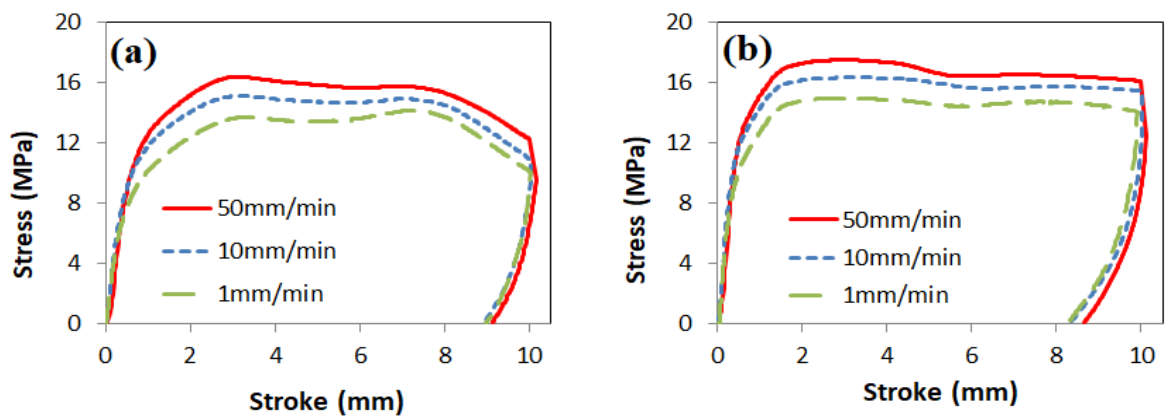

Figure 3-5 Typical stress-stroke curves generated from the indentation loading, using an indenter of 7mm (a) and 13mm (b) in diameter for different loading speeds, both to the stroke of 10mm at 23°C.

3.4.2 FE Results

As stated in section 3.3, material parameters in Equations (3.1) to (3.6) were adjusted in an iterative process to achieve a good agreement between outputs from the FE models and results from the experimental testing. *Table 3-2* gives an example of values for these parameters using the 13mm indenter at the loading speed of 10mm/min. Note that ε_{ti} in *Table 3-2*, with i = 1 to 8, represents the maximum strain for section i. The elastic modulus for each indenter size and loading speed was obtained by fitting the initial linear part of the stress-stroke curve obtained from the experimental testing. *Table 3-2* indicates that parameters for the equations before the necking, i.e. for Equations (3.1-a) to (3.1-b), are same among the base, creep and damage models. This is because creep or damage was not considered before the onset of the necking. After creep or damage is activated, values for the corresponding parameters become different among the three models. The deep drawing process that generated a truncated cone in the specimen occurred in the strain range for Equation (3.1-d) which as shown in *Table 3-2* includes 8 sections. However, not all of the 8 sections were used in the FE modelling, as the strain generated in the models might not reach the maximum range given in *Table 3-2* when the stroke reached 10mm. The last two rows in *Table 3-2*, for creep and damage parameters, are to govern creep and damage development in the creep and damage models, respectively.

Figure 3-6 summarizes stress-stroke curves from the FE models using 7 and 13mm indenters at three loading speeds. Each figure contains a curve from the experimental testing (dash lines) and three curves generated from the FE simulation using the base model, the creep model, and the damage model. As shown in this figure, the curve profile for the entire loading stage can be mimicked by all 3 FE models. Even the base model, without the explicit consideration of damage evolution or creep deformation, can mimic the stress drop after the stroke of 8mm using the 7mm indenter. Similarly, creep and damage models can also mimic the stress drop after the stroke of 8mm. Since it was not possible to apply both creep and damage simultaneously, creep deformation and damage evolution were introduced to different FE models, to result in the three models, which can all mimic the stress-stroke curves obtained experimentally. As to be shown later, using input equivalent stress-strain curves from the three models, stress drop caused by creep deformation and damage evolution can be extracted from the three models, and the equivalent stress-strain curves, without creep or damage, can be compared for deformation introduced by 7 and 13mm indenters.

Figure 3-7 summarizes input equivalent stress-strain curves, i.e. Equation (3.1), for all test conditions considered in this study. These input curves were established for the three FE models described in Section 3.3. The maximum strain for each curve is equal to the maximum strain that the model experienced in the indentation test. For each model, material properties, i.e. Young's modulus and Poisson's ratio, stress-strain relationship in the plastic regime, time-hardening creep, and adjustable damage variables, are determined in order for the FE models to generate the output that fits results from the experimental testing. As discussed in Section 3.3, Finite element simulation, the input equivalent stress-strain curves for the base model include the influence by damage and creep, but the corresponding curves for the creep model include only the influence by damage, as the influence by creep was separately considered using a power law creep function, Equation (3.2). Conversely, the input equivalent stress-strain curves for the damage model include only the influence by creep, as the influence by damage was considered using a damage evolution function, Equation (3.6). As shown in *Figure 3-7*, at a given loading speed and for a given indenter size, the input equivalent stress-strain curve for the base model is the lowest, as the curve includes stress drop caused by both creep and damage. Difference of the curves in *Figure 3-7* for creep or damage model from that for the base model represents the stress drop caused by the creep or damage, respectively.

Table 3-2 Values for parameters and strain range in Equations (3.1) to (3.6), determined from the FE simulation.

FE model			Loading speed of 10 mm/min		
			Base model	Creep model	Damage model
Equation 1(a)		ε_y	0.005	0.005	0.005
		E	1000	1000	1000
		ν	0.4	0.4	0.4
Equation 1(b)		ε_n	0.1	0.1	0.1
		a	30.02	30.02	30.02
		b	0.01	0.01	0.01
		c	0.04	0.04	0.04
		d	-12.055	-12.055	-12.055
		e	18.844	18.844	18.844
Equation 1(c)		ε_t	0.2	0.2	0.2
		α_k	26.51031	26.57	26.57
		N	0.00005	0.001	0.001
Equation 1(d)	Section 1	ε_{t1}	0.5	0.6	0.55
		K_1	26.00833	26.3	26.5
		M_1	0.05	0.05	0.05
		β_1	0.6	0.6	0.6
	Section 2	ε_{t2}	0.8	0.8	0.8
		K_2	24.35	23.56	23.56
		M_2	0.15	0.2	0.2
		β_2	0.6	0.6	0.6
	Section 3	ε_{t3}	1.1	1.1	1.1
		K_3	15.053	13.94	13.94
		M_3	0.7	0.8	0.8
		β_3	0.6	0.6	0.6
	Section 4	ε_{t4}	1.4	1.4	1.4
		K_4	8.866	8.21	10.153
		M_4	1.2	1.3	1.1
		β_4	0.6	0.6	0.6
	Section 5	ε_{t5}	1.7	1.7	1.7
		K_5	11.325	8.21	8.99
		M_5	1	1.3	1.2
		β_5	0.6	0.6	0.6
	Section 6	ε_{t6}	2	2	2
		K_6	3.771	3.59815	5.19
		M_6	1.8	1.9	1.6
		β_6	0.6	0.6	0.6
	Section 7	ε_{t7}	3	3	3
		K_7	1.7675	2.65722	1.544
		M_7	2.3	2.1	2.4
		β_7	0.6	0.6	0.6
	Section 8	ε_{t8}	4	4	4
		K_8	1.457	2.19014	1.273
		M_8	2.4	2.2	2.5
		β_8	0.6	0.6	0.6
Creep Properties		$A\times10^{15}$		6.6	
		n		7.8	
		m		-0.9	
Damage Properties		ε_f^{pl}			0.2
		θ_s			0.47
		$\dot{\varepsilon}^{pl}$			0.04348
		u^{pl}			12
		α			3

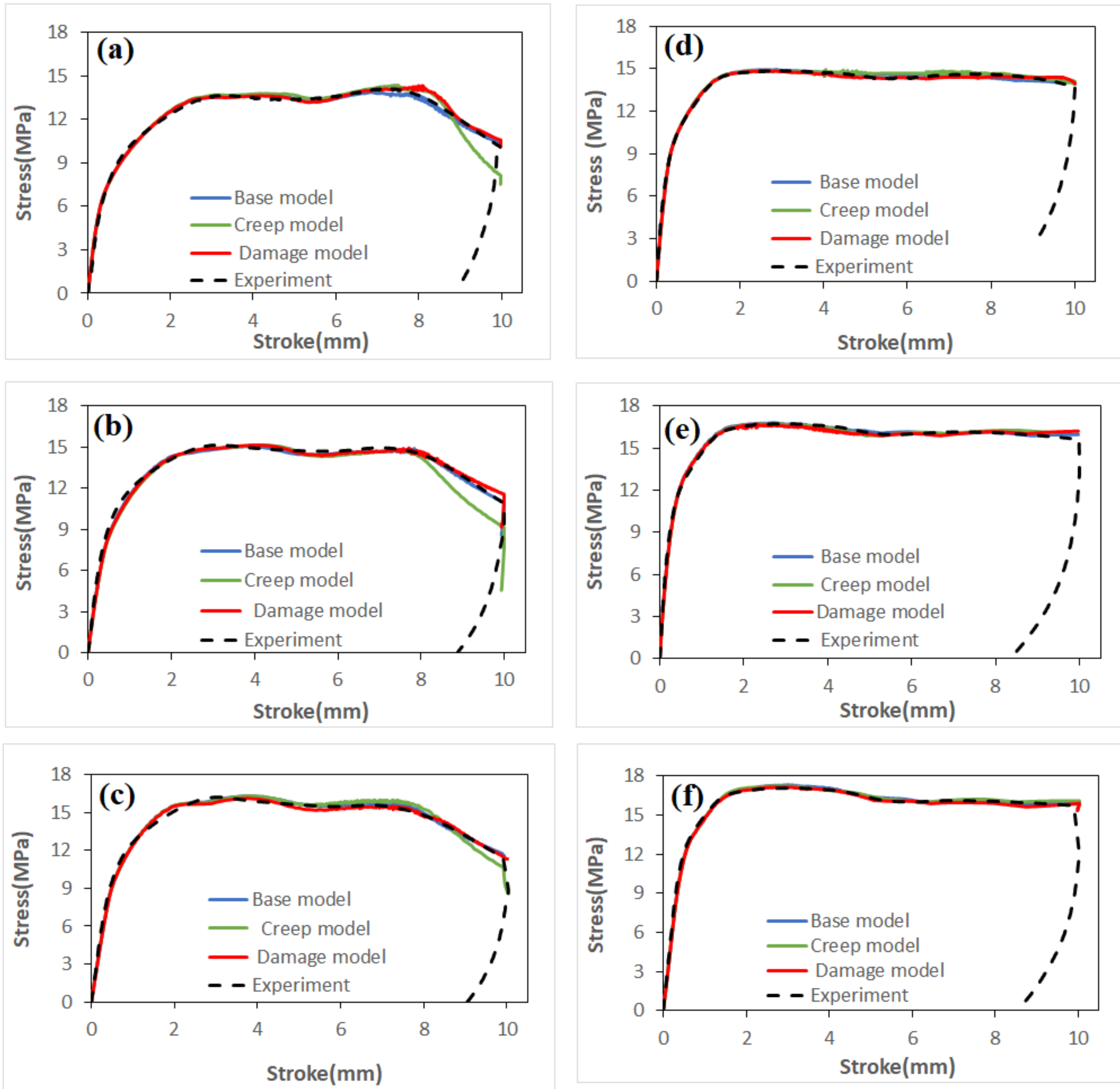

Figure 3-6 Comparison of stress-stroke curves from experiment with those from base model, the creep model and the damage model: (a), (b) and (c) for 7mm indenter and (d), (e) and (f) for 13mm indenter.

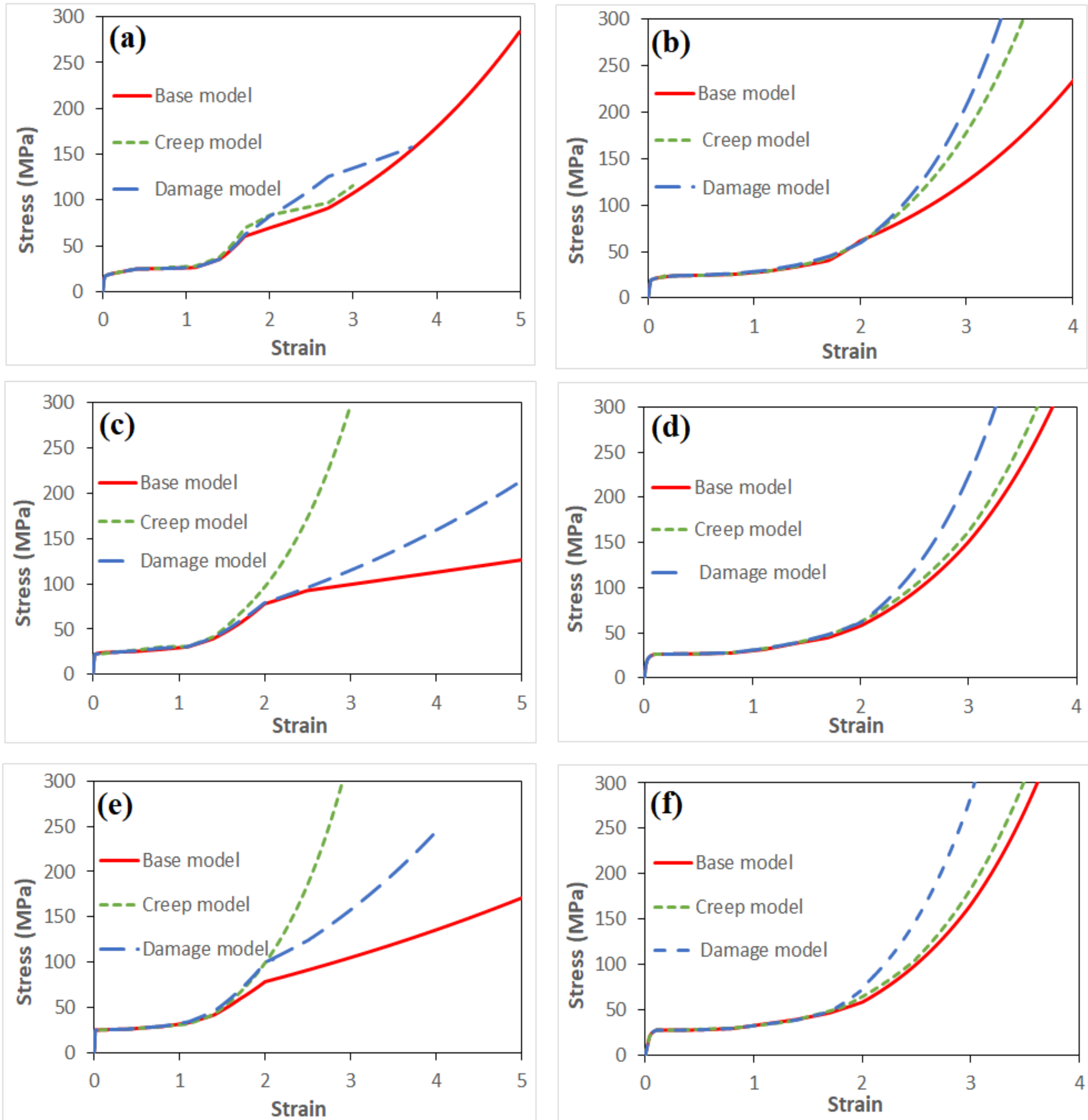

Figure 3-7 Input equivalent stress-strain curves established by adjusting parameters in Equations (3.1) to (3.6) for base model, creep model, and damage model: (a) and (b) using the indenter of 7 and 13mm respectively at loading speed of 1mm/min, (c) and (d) using the indenter of 7 and 13mm respectively at loading speed of 10mm/min and (e) and (f) using the indenter of 7 and 13mm respectively at loading speed of 50mm/min.

Figure 3-8 presents the stress drops by creep and damage during the indentation test, that is, *Figure 3-8 (a)* and *(c)* for 7mm indenter and *(b)* and *(d)* for 13mm indenter. The stress drop due to creep deformation is obtained by subtracting the input equivalent stress-strain curve for the base model from the counterpart for the creep model, as shown in *Figure 3-8 (a)* and *(b)* for 7mm and 13mm indenters, respectively. Likewise, the stress drop due to damage is obtained by subtracting the input equivalent stress-strain curve for the base model from the counterpart for the damage model, as shown in *Figure 3-8 (c)* and *(d)* for 7mm and 13mm, respectively. Each figure contains three curves, for different loading speed used for the testing. Since the strain range generated from the test varies with the loading speed, curves in *Figure 3-8* cover different strain ranges. For each indenter with the increase of the loading speed, the damage-generated stress drop is more intensified. By adding stress drops shown in *Figure 3-8 (a)* to *(d)* to the corresponding equivalent stress-strain curve for the base model of the same indenter in *Figure 3-8 (a)* to *(e)*, the equivalent stress-strain curves without stress drop by creep or damage are established, as shown in *Figure 3-8 (e)* and *(f)*.

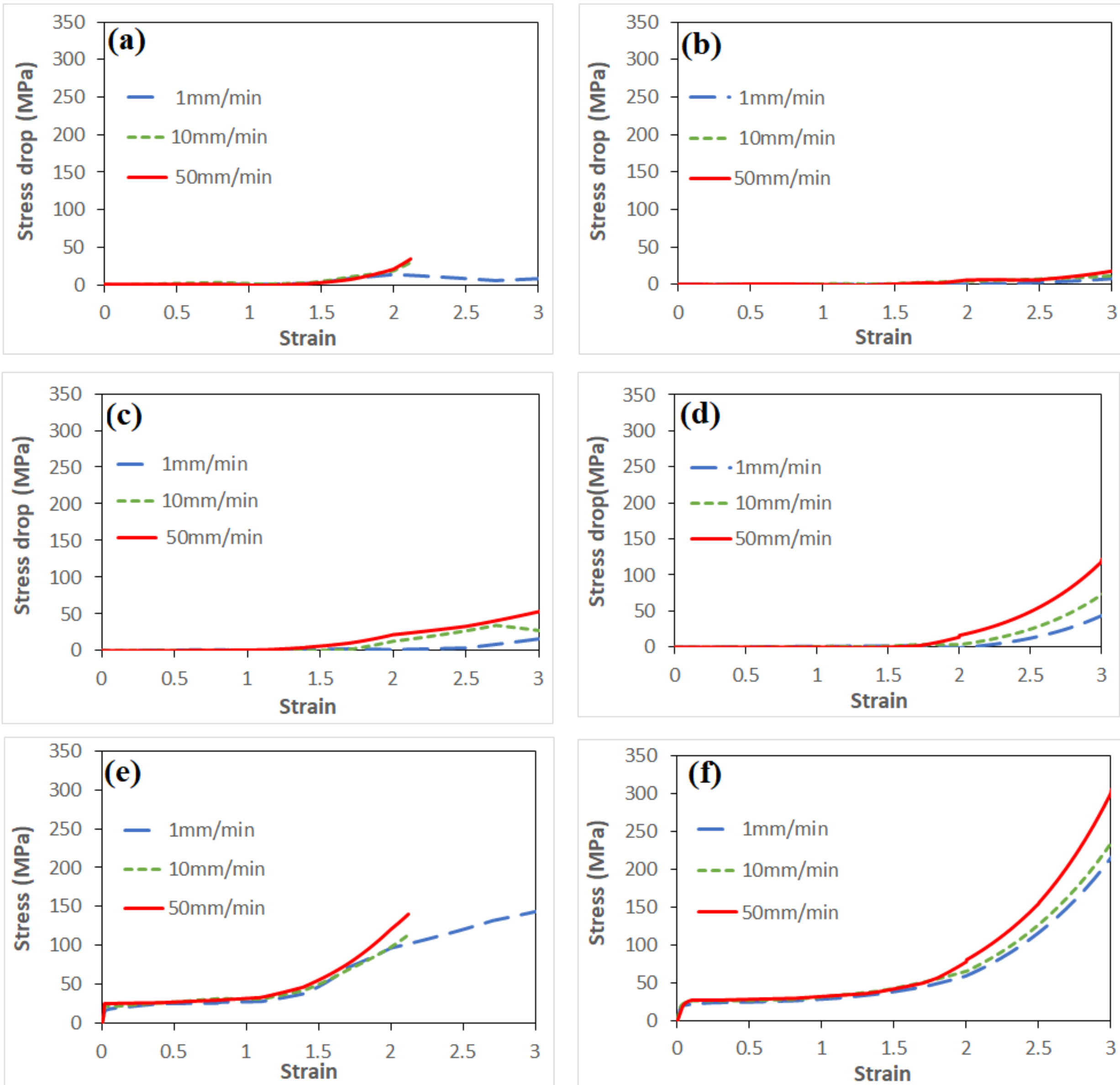

Figure 3-8 Summary of stress drop derived from results from Figure 7: (a) and (b) due to creep deformation using 7mm and 13mm indenters, respectively, (c) and (d) due to damage evolution using 7mm and 13mm indenters respectively, (e) and (f) stress-strain relationship without creep or damage using 7mm and 13mm indenters, respectively.

Figure 3-9 presents contour plots of von Mises stress in the deformation process, using the base model with indenters of 7 and 13 mm for the left and right contour plots, respectively. The contour plots correspond to strokes in the range of 2-10mm at the loading speed of 10mm/min. A magnified view at a highly stretched location is also included in each plot. Plots *(a)* and *(b)* are for the stroke of 2mm using 7mm and 13mm indenters, respectively. Contour plots at this stroke indicate that local stretch has started using the 13mm indenter, as the upper surface of PE specimen starts contacting with the cylindrical surface of the indenter. It should be noted that the corresponding curves in *Figure 3-6*, *(b)* and *(e)* for 7mm and 13mm indenters, respectively, indicate that necking should have started in the model with 13mm indenter, but yet to occur in the model with 7mm indenter. *Figure 3-9 (c)* and *(d)* indicate that at the stroke of 4mm, both indenters have introduced the deep drawing. The rest of the contour plots in *Figure 3-9*, *(e)* to *(h)*, show the development of localized stretch by both indenters to form a truncated cone, as shown in *Figure 3-3 (b)*, with stress drop occurring in other regions of the models. *Figure 3-9* suggests that the localized stretch started around the region in contact with the bottom circumference of the indenter and results in a truncated cone shape with the highest stretch on the inner surface. Comparison of the contour plots between *Figure 3-9 (g)* and *(h)* indicates that the localized stretch generates a wide range of stress and strain distribution in the models. Therefore, at a given stroke, more than one expression in Equation (3.1) should be involved in the modelling, which complicates the iteration process significantly for determining parameter values for the constitutive equations, such as those shown in *Table 3-2*.

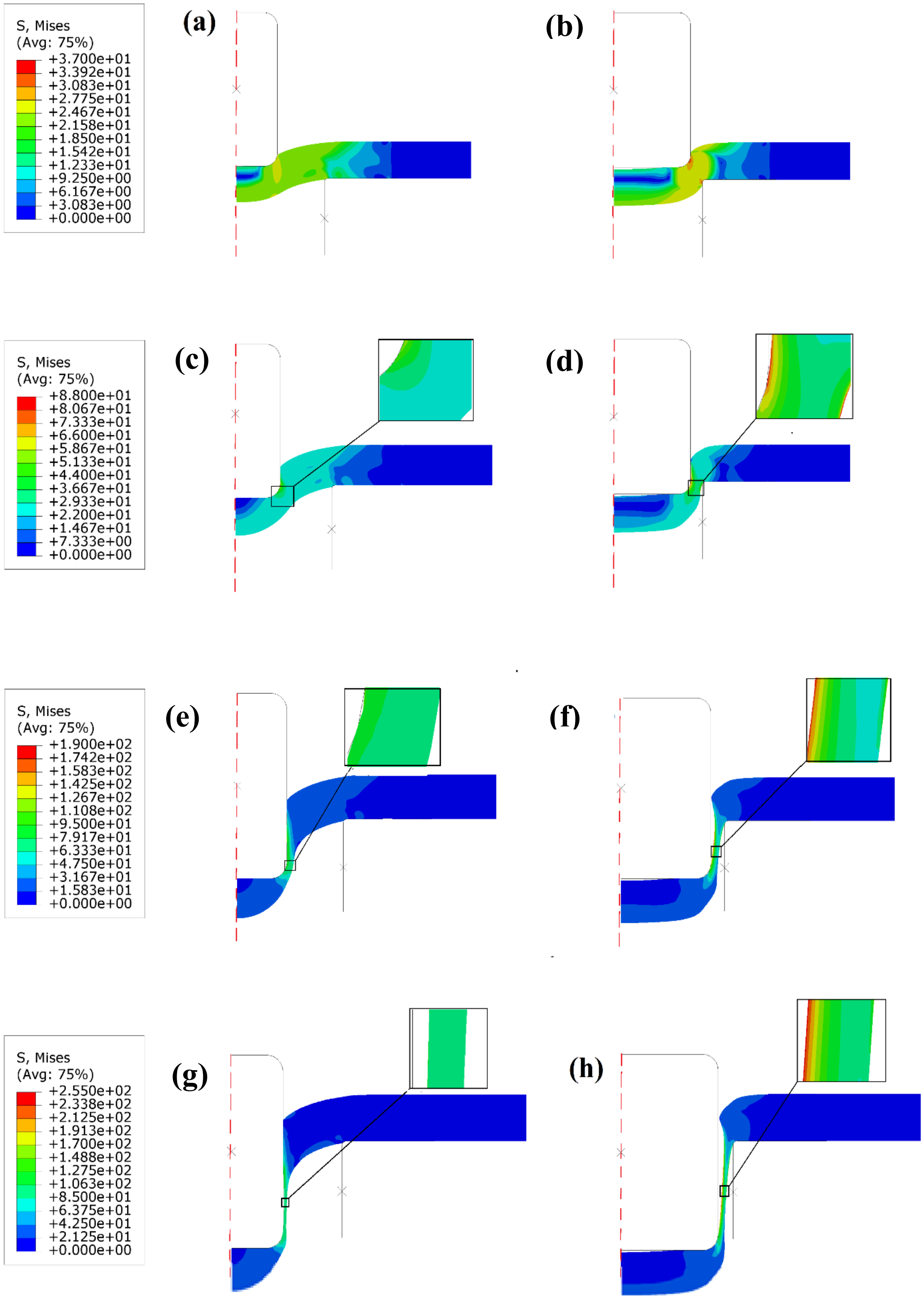

Figure 3-9 Comparison of equivalent stress contour plots for 7 and 13mm indenters with elastic-plastic material properties at the loading speed of 10 mm/min, at the stroke of 2mm (a) and (b), 4mm (c) and (d), 7mm (e) and (f), and10mm (end of the loading stage) (g) and (h).

Figure 3-10 summarizes variation of the minimum thickness on the highly stretched regions of FE models in *Figure 3-9*, plotted as a function of the indenter stroke. The figure suggests that the final thickness generated by the two indenters is about the same, but the 13mm indenter introduced a slightly higher rate of the thickness reduction than the 7mm indenter at the stroke up to 4mm, and after the stroke of 6mm, the thickness change introduced by both indenters is at a much slower rate, to generate similar values for the minimum thickness in the truncated cone. Even though the minimum thickness in the truncated cone is similar by the two indenters, the magnified views in *Figure 3-9* suggest that the gap between the indenter surface and the inner surface of the truncated cone generated by the 13mm indenter is less than that by the 7mm indenter.

Variation of the maximum principal stress in an element that is located in the middle of the highly stretched region has been examined using the base model at the loading speed of 10mm/min, to investigate the effect of indenter size on the stress response to the deformation. *Figure 3-11(a)*

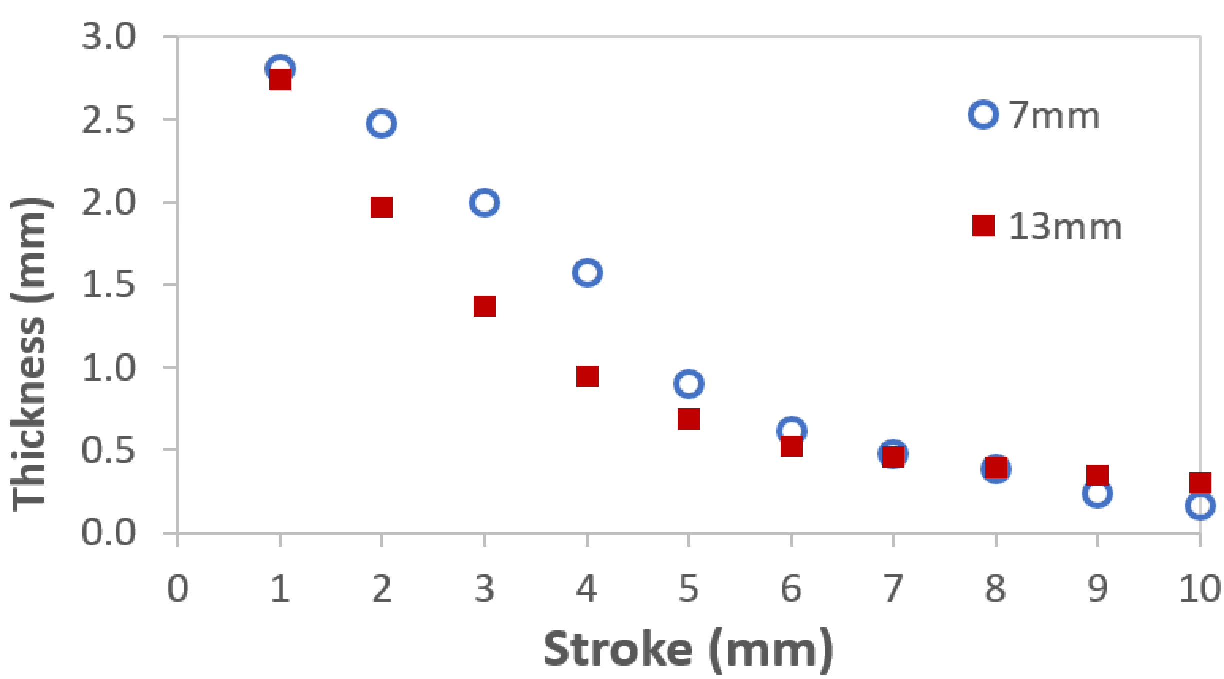

Figure 3-10 Minimum thickness measured from the FE models at strokes in the range from 1 to 10mm for 7 and 13mm indenters using the base model, at the loading speed of 10 mm/min.

presents the variation as a function of stroke, and *Figure 3-11(b)* shows the location of the element. *Figure* 3.11 *(a)* indicates that the stroke for the transition of the maximum principal stress from negative to positive is for the start of the deep drawing. For the 7mm indenter, the maximum principal stress is negative till the stroke reaches around 4 mm, suggesting that the deep drawing starts around that stroke level. For the 13mm indenter, on the other hand, the stretch starts much earlier, as the maximum principal stress becomes positive at a stroke below 2mm. This is consistent with the results shown in *Figure 3-9* where at 4mm stroke, deep drawing has clearly commenced for the 13mm indenter but not for the 7mm indenter. For most of the stroke range, stress level generated by the 13mm indenter is higher than that by the 7mm indenter. For the other two FE models (creep and damage models), the outputs show the similar results and trends. Overall, the total deformation process for both indenters could be described by a two-stage process, bending and deep drawing. Bending occurs before the stroke of 4mm for the 7mm indenter, after which the specimen enters the deep drawing stage. For the 13mm indenter, the bending stage is very small, up to a stroke of less than 2mm, and deep drawing occurred in the remaining stroke of the test. Note that the model output may not be sensitive enough to reflect the change of stress state in one element. However, we have chosen the element in the mid thickness of the high stretched region in order to provide a conservative comparison of the stress response to stroke between the two indenters.

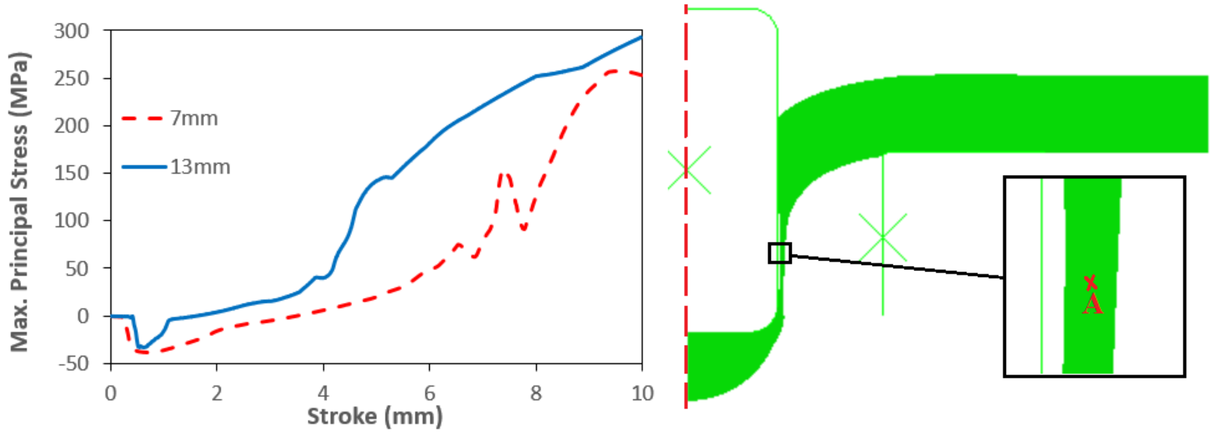

(a) **(b)**

Figure 3-11 Output of the maximum principal stress from an element in the highly stretched region: (a) plotted as a function of stroke, and (b) location of the element, as indicated by A.

Figure 3-12 compares curves for the output of the von Mises stress versus stroke from a specific element in the highly stretched region, which experiences the largest strain in the model. *Figure 3-12* suggests that for the 13mm indenter (i.e. plots *(d)* to *(f)*) the curves show a largely monotonic increase of stress with the increase of stroke, while for the 7mm indenter, a significant stress fluctuation occurs in the stroke range from 6 to 8mm. Such a stress fluctuation is likely to cause relaxation of polymer molecules to allow recrystallization. Therefore, some crystalline structures could be regenerated after being destroyed by the deep drawing, to reduce effectiveness of using the deep drawing to convert the crystalline phase to the amorphous phase. Since increase of the amorphous phase is expected to reduce the time for ESC development when the specimen is exposed to a chemical agent, the 13mm indenter should be more suitable than the 7mm indenter used in the new test to characterize ESCR for PE (i.e. to initiate crack earlier). This expectation is consistent with that shown in *Figure 3-8 (c)* and *(d)* in which stress drop due to damage by the 13mm indenter is more than that by the 7mm indenter.

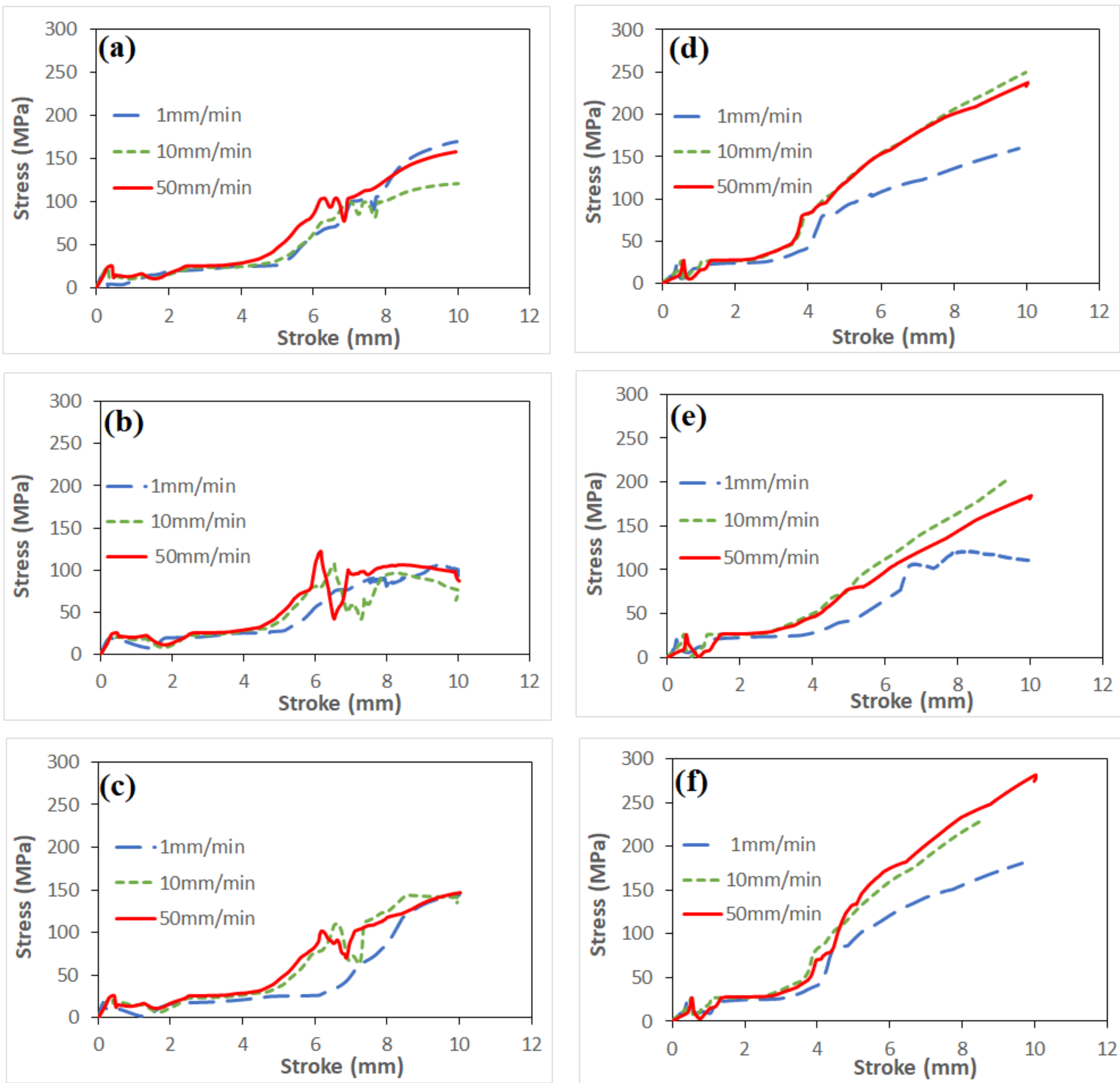

Figure 3-12 Output stress-stroke curves from the FE models at the loading speeds of 1, 10, and 50mm/min for a 7mm indenter using (a) based model, (b) creep model, and (c) damage model, and for a 13mm indenter r using (d) base model, (e) creep model, and (f) damage model.

3.5 Conclusions

Work presented in this paper is part of a study to develop a new indentation test to characterize ESCR for PE. The test setup includes an indenter that applies a transverse loading to a plate specimen, and a container to house an aggressive agent to generate crack on the deformed specimen. The work investigated specimen deformation at the loading stage, to examine the stress-strain relationship in PE when subjected to indenter of different size at different loading speeds. An axi-symmetric finite element model was developed to mimic the stress-stroke relationship generated by the indentation loading. Three FE models, namely base model, creep model and damage model, were used to mimic the stress-stroke curves collected from the experimental testing. Then, based on the FE models, influence of indenter size on the stress drop by creep and damage in the testing is investigated using the equivalent stress-strain input data for these models. In addition, the stress-strain relationship without damage or creep are established from input stress-strain curves for the three models. The study concludes that for the given indenter size at different loading speeds, even without damage or creep, higher loading speed generates higher stress response to deformation and the 13mm indenter introduces more damage in the PF and is better than the 7mm indenter for the ESCR characterization of PE.

Acknowledgement

The work was sponsored by Natural Sciences and Engineering Research Council of Canada (NSERC), and Imperial Oil, the University Research Awards program.

References

[1] R.K. Krishnaswamy, Analysis of ductile and brittle failures from creep rupture testing of high-density polyethylene (HDPE) pipes, Polymer 46 (2005) 11664–11672.

<http://www.sciencedirect.com/science/article/pii/S0032386105014473>.

[2] N. Kiass, R. Khelif, L. Boulanouar, K. Chaoui, Experimental approach to mechanical property variability through a high-density polyethylene gas pipe wall, J. Appl. Polym. Sci. 97 (2005) 272–281, <http://dx.doi.org/10.1002/ app.21713/abstract> (Copyright _ 2005 Wiley Periodicals, Inc.).

[3] F. Hasan, J. Iqbal, F. Ahmed, Stress corrosion failure of high-pressure gas pipeline, Eng. Fail. Anal. 14 (2007) 801–809.

<http:// www.sciencedirect.com/science/article/pii/S1350630706001506>.

[4] M.A.L. Hernández-Rodríguez, D. Martínez-Delgado, R. González, A. Pérez Unzueta, R.D. Mercado-Solís, J. Rodríguez, Corrosive wear failure analysis in a natural gas pipeline, Wear 263 (2007) 567–571. <http://www.sciencedirect.com/science/article/pii/S0043164807004590>.

[5] H.M. Shalaby, W.T. Riad, A.A. Alhazza, M.H. Behbehani, Failure analysis of fuel supply pipeline, Eng. Fail. Anal. 13 (2006) 789–796.

<http://www.sciencedirect.com/science/article/pii/S1350630705000907>.

[6] C.R.F. Azevedo, Failure analysis of a crude oil pipeline, Eng. Fail. Anal. 14 (2007) 978–994. <http://www.sciencedirect.com/science/article/pii/S135063070600210X>.

[7] Z.A. Majid, R. Mohsin, Z. Yaacob, Z. Hassan, Failure analysis of natural gas pipes, Eng. Fail. Anal. 17 (2010) 818–837.

<http://www.sciencedirect.com/science/article/pii/S1350630709002532>.

[8] A. Lustiger, Understanding environmental stress cracking in polyethylene. In: Portnoy RC, editor. Medical plastics: degradation, resistance & failure analysis, Medical Plastics, 1998, p. 66-71.

[9] DC Wright, Environmental stress cracking of plastics. Shawbury, UK: Smithers Rapra Technology Ltd; 1996.

[10] EJ. Kramer. Developments in polymer fracture. London, England: Applied Science Publishers; 1979.

[11] W. Brostow, R.D.Corneliussen. Failure of Plastics. Munich, New York: Hanser Pub; 1989.

[12] J.Scheirs. Compositional and failure analysis of polymers: A practical approach, Wiley, Chichester; 2000, p.556-561.

[13] L. Kurelec L, M. Teeuwen, H. Schoffeleers, R. Deblieck. Strain hardening modulus as a measure of environmental stress crack resistance of high-density polyethylene. Polymer. 2005; 46(17):6369-6379. < https://www.sciencedirect.com/science/article/abs/pii/S0032386105006555>.

[14] J. Cheng, M. Polak, A. Penlidis. A tensile strain hardening test indicator of environmental stress cracking resistance. J Macromol Sci Pure and Applied Chemistry. 2009; 45(8): 599-611. <https://www.tandfonline.com/doi/abs/10.1080/10601320802168728>.

[15] MJ. Cawood, AD. Channell, G. Capaccio. Crack initiation and fibre creep in polyethylene. Polymer. 1993; 34(2): 423-425.

<https://www.sciencedirect.com/science/article/abs/pii/003238619390100O>.

[16] LJ. Rose, AD. Channell, CJ. Frye, G. Capaccio. Slow crack growth in polyethylene: a novel predictive model based on the creep of craze fibrils. J Appl Polym Sci.1994; 54(13): 2119-2124.

<https://onlinelibrary.wiley.com/doi/abs/10.1002/app.1994.070541314>.

[17] A.D. Drozdov, J.d. Christiansen, Creep failure of polypropylene: experiments and constitutive modeling, Int. J. Fract. 159 (2009) 63–79. <http://link.springer.com/article/10.1007/s10704-009-9384-x>.

[18] T.H. Hyde, W. Sun, J.A. Williams, Life estimation of pressurised pipe bends using steady-state creep reference rupture stresses, Int. J. Press. Vessels Piping, 2002, 79: 799–805. <http://www.sciencedirect.com/science/article/pii/S0308016102001345>.

[19] J.P. Rouse, W. Sun, T.H. Hyde, A. Morris, Comparative assessment of several creep damage models for use in life prediction, Int. J. Press. Vessels Piping, 2013, 108–109 :81–87. <http://www.sciencedirect.com/science/article/pii/S0308016113000689>.

[20] G.J. Frank, R.A. Brockman, A viscoelastic–viscoplastic constitutive model for glassy polymers, Int. J. Solids Struct, 2001. 38: 5149–5164.

<http://www.sciencedirect.com/science/article/pii/S0020768300003395>.

[21] J. Betten, S. Sklepus, A. Zolochevsky, A microcrack description of creep damage in crystalline solids with different behaviour in tension and compression, Int. J. Damage Mech. 8 (1999) 197–232. <http://ijd.sagepub.com/content/8/3/197>.

[22] J. Dufailly, J. Lemaitre, Modeling very low cycle fatigue, Int. J. Damage Mech, 1995, 4:153–170. <http://ijd.sagepub.com/content/4/2/>.

[23] J.A. Alvarado-Contreras, M.A. Polak, A. Penlidis, Constitutive modeling of damage evolution in semicrystalline polyethylene, J. Eng. Mater. Technol, 2010, 132: 041009. <http://materialstechnology.asmedigitalcollection.asme.org/article.aspx?articleid=1428770>.

[24] Y. Zhang, P.Y. Ben Jar, Phenomenological modelling of tensile fracture in PE pipe by considering damage evolution, Materials and Design, 77 (2015) 72-82.

<https://www.sciencedirect.com/science/article/abs/pii/S026130691500179X >.

[25] P.Y.B. Jar, A New Concept of using Transverse Loading to Characterize Environmental Stress Cracking Resistance (ESCR) of Polyethylene (PE), Res Dev Material Sci, 3(5), 2018. <https://crimsonpublishers.com/rdms/pdf/RDMS.000574.pdf>.

[26] B. Jar, P.Ward, Ch.Jar, Y.Zhang. A New Method to Characterize Environmental Stress Cracking Resistance (ESCR) of Polyethylene (PE) and its Pipes, in: ANTE 2017 The Plastic Technology Conference, Anaheim California, 2017.

<https://www.semanticscholar.org/paper/A-NEW-METHOD-TO-CHARACTERIZE-ENVIRONMENTAL-STRESS-(-Jar-Ward/4211243cddfa5b894022b9c1b1f15e311a36316f>

[27] ASTM D732-17, Standard Test Method for Shear Strength of Plastics by Punch Tool, ASTM International, West Conshohocken, PA, 2017. < https://www.astm.org/Standards/D732.htm>

[28] S. Dhouibi, M. Boujelbene, M, Kharrat, M, Dammak, A, Maalej, Friction Behavior of High-Density Polyethylene (HDPE) Against 304L Steel: An Experimental Investigation of the Effects of Sliding Direction, Sliding History and Sliding Speed, Journal of Surfaces and Interfaces of Materials, 2013; 1(1): 71–76. < https://www.ingentaconnect.com/content/asp/jsim>

[29] I. H.J.Kwon, P.-Y. Ben Jar. On the application of FEM to deformation of high-density polyethylene. International Journal of Solids and Structures, 2008,45(11-12):3521-3543. < https://www.sciencedirect.com/science/article/pii/S0020768308000796>

[30] S. Muhammad, P.Y.B. Jar, Effect of aspect ratio on large deformation and necking of polyethylene, J. Mater. Sci. 2011, 46, 1110–1123.

<https://www.sciencedirect.com/science/article/pii/S0020768308000796>

[31] P.-Y. Ben Jar, S. Muhammad, Cavitation-induced rupture in high-density polyethylene copolymers, Polymer Engineering & Science. J, 2011,52:1005–1014.

<https://onlinelibrary.wiley.com/doi/abs/10.1002/pen.22169 >

[32] S. Muhammad, P.-Y.B. Jar. Determining stress–strain relationship for necking in polymers based on macro deformation behavior, Finite Elements in Analysis and Design. J, 2013, 70–71: 36–43. < https://www.sciencedirect.com/science/article/abs/pii/S0168874X13000449 >

[33] G. Ayoub, F. Zaïri, M. Naït-Abdelaziz, J.M. Gloaguen, Modelling large deformation behaviour under loading–unloading of semicrystalline polymers: application to a high density polyethylene, Int. J. Plast, 2010. 26: 329–347.

<http://www.sciencedirect.com/science/article/pii/S0749641909000928>.

[34] K. Hong, A. Rastogi, G. Strobl, A model treating tensile deformation of semi crystalline polymers: quasi-static stress_strain relationship and viscous stress determined for a sample of polyethylene, Macromolecules, 2004, 37:10165–10173, http://dx.doi.org/10.1021/ma049174h.

[35] D.J. Celentano, J.-L. Chaboche, Experimental and numerical characterization of damage evolution in steels, Int. J. Plast, 2007, 23:1739–1762.

<http://www.sciencedirect.com/science/article/pii/S0749641907000484>.

[36] F. Detrez, S. Cantournet, R. Seguela, Plasticity/damage coupling in semicrystalline polymers prior to yielding: micromechanisms and damage law identification, Polymer, 2011, 52 :1998–2008. <http://www.sciencedirect.com/science/article/pii/S0032386111002023>.

[37] G. Gu, Y. Xia, C.-h. Lin, S. Lin, Y. Meng, Q. Zhou, Experimental study on characterizing damage behavior of thermoplastics, Mater. Des. 44 (2013) 199–207.

<http://www.sciencedirect.com/science/article/pii/S0261306912005146>.

[38] ABAQUS Advanced Topics. Material Damage and Failure. <https://imechanica.org/files/19-damage-failure.pdf>; 2005

[39] S. Humbert, O. Lame, J.M. Chenal, C. Rochas, G. Vigier, New insight on

initiation of cavitation in semicrystalline polymers: in-situ SAXS measurements, Macromolecules, 2010, 43:7212–7221. <http://dx.doi.org/ 10.1021/ma101042d>.

[40] K. Schneider, S. Trabelsi, N.e. Zafeiropoulos, R. Davies, C. Riekel, M. Stamm, The study of cavitation in HDPE using time resolved synchrotron X-ray scattering during tensile deformation, Macromol. Sympos,2006. 236:241–248, http://dx.doi.org/10.1002/masy.200690062/abstract (Copyright _ 2006WILEY-VCH Verlag GmbH & Co. KGaA, Weinheim).

[41] J.C. Viana, Structural interpretation of the strain-rate, temperature and morphology dependence of the yield stress of injection molded semicrystalline polymers, Polymer 46 (2005) 11773–11785. <http:// www.sciencedirect.com/science/article/pii/S0032386105014710>.

Chapter 4

4. Summary and future works

This chapter summarizes the main contributions of this research work and suggests possible work for the future investigation.

4.1. Summary of contributions

Polyethylene (PE) are being increasingly used as a pipe material for natural gas and water transportation. Damage generated during installation or maintenance processes such as squeeze-off causes mechanical property degradation of the pipe, thus reducing its remaining service life. The other major types of PE failure, known as environmental stress cracking (ESC), can be accrued over the time. This brittle failure type happens when PE pipes are in contact with an environment that contains aggressive agent. Because of the potentials of pipeline failure for the huge economic losses and threats to the public safety, it is extremely important to have a tool to characterize the likelihood of pipeline failure.

This thesis focuses on the characterization of mechanical properties of PE in the above two conditions (i.e. squeeze off and ESC) through developing FE simulation models. One case is for PE pipe under the squeeze off process. The time-dependent behaviour of PE was considered using a creep model. This case is to use a set of squeeze-off test results that were conducted in a previous study to explore the possibilities of determining the stress-strain relationship to improve the simulation accuracy. The other case is to subject PE to a transverse loading. This is a part of a test setup developed to apply transverse loading to a plate specimen to generate deep drawing. With a container that includes an aggressive agent, cracks can be generated from the deformed specimen surface. The test results at the loading stage were used to explore the possibilities of determining the stress-strain relationship in the PE specimen. The material characterization considered three different scenarios, i.e. without any explicit expression for damage or creep development (base model), with an explicit expression for creep (creep model), and with an explicit expression for damage (damage model).

The pertinent research work presented in this thesis is summarized below.

(1) Material sensitivity analysis in a cylindrical model

The material constitutive equation used in this study included different expressions for different strain ranges. In each expression there are some adjustable parameters. This step was developed to identify fitting parameters in the constitutive equation which have a bigger influence on the output results than the other parameters. An axisymmetric cylinder model of constant cross section, subjected to tensile displacement, was used for this purpose. Sensitivity of the stress output to the change of parameter values was analyzed to determine the most sensitive parameters. The parameters which are the most influential parameters for adjusting the output stress were determined, and thus improving the closeness of the simulation results with the experimental measurements.

(2) Effects of Squeeze-off on Mechanical Properties of Polyethylene Pipes

Influence of the squeeze-off process, a popular procedure for pipe maintenance or repair, on PE's mechanical properties has been investigated, with a special attention to the effect of squeezing speed. The experimental results which were recently conducted, was used to develop a three-dimensional FE model which facilitated the determination of strain and strain rate in the pipe wall during the squeeze-off process. The FE simulation shows that the constitutive equation can provide suitable stress-strain relationship to mimic closely the squeeze-off process. Moreover, the results suggest that due to plastic deformation, the pipe cannot return completely to its initial dimensions. As a result, significant degradation could be introduced by the squeeze-off process.

(3) Finite Element Modelling of Deep Stretch of Polyethylene Plate under Indentation Loading

This part of thesis presents a study that uses indentation loading to generate deep stretch of PE, which is part of a project to design a new test method to shorten the time for crack initiation during the exposure to an aggressive agent in order to accelerate the pace for characterizing PE's environmental stress cracking resistance (ESCR). Two cylindrical indenters of 13 and 7mm in diameter were used to generate the deep stretch in the central part of a circular area of 15mm in diameter. The study uses finite element (FE) modelling to establish stress variation and distribution during the deep stretch, but without the exposure to the aggressive agent. Three types of material input data were considered, one purely based on elastic-plastic (EP) deformation (based model), another including damage generation (damage model), and the third including creep deformation (creep model), all of which have the input stress-strain curve calibrated by regenerating the load-stroke curve obtained from the experimental testing. Comparison of the input stress-strain curves for the three types of FE modelling reveals that the stress drops due to damage and creep, and their differences caused by the indenter size and loading speed used for the testing. The three types of input stress-strain curves also led to establishment of a stress-strain relationship for PE when no damage or creep generated in the deformation, which suggests that the stress-strain curve is more sensitive to the loading speed using the 7mm indenter. The FE modelling using 7mm indenter also shows more frequent stress relaxation during the deep drawing than the 13mm indenter. Therefore, the study concludes that the 13mm indenter is much more effective than the 7mm indenter in transforming the crystalline phase to the amorphous phase through the deep drawing, and is expected to provide measurement of ESCR with less scattering.

4.2. Future work

The research work presented in this thesis is a step towards developing an approach to predict the mechanical behaviour of PE pipe in different environment. However, further research is needed to examine other possible scenarios.

(1) Characterization of damage development under different loading conditions

The proposed FE model has been successfully used to determine damage evolution under the transverse loading. In order to obtain the damage evolution under this loading condition, the method could be extended to study the damage behavior under fatigue or creep loading. In addition, the experimentally measured damage evolution law can be implemented in FE models to study fracture behaviors of PE pipe.

(2) Simultaneous effects of damage and creep in PE

In this thesis since the ABAQUS does not allow simultaneous consideration of creep deformation and damage evolution, the creep and damage evolution have to be considered separately. Using a UMAT script, it is possible to consider both creep and damage at the same time. This method can be used with an elastic-plastic model at the same time to include all the possible material behaviour for PE.

(3) Development of mathematical models to determine ESCR of PE using FE results of the deep drawing of PE

In this thesis, a model was presented to study the use of indentation loading to generate deep drawing of PE, which is part of a project to design a new test method to shorten the time for crack initiation during the exposure to an aggressive agent, in order to accelerate the pace for characterizing PE's environmental stress cracking resistance (ESCR). The mathematical models can be developed to use the FE results as an input to investigate the time for crack initiation on the deformed PE. The model can then be used to investigate influence of different factors on the ESC development, to make the results useful for the industry applications.

Bibliography

ABAQUS Advanced Topics. Material Damage and Failure. <https://imechanica.org/files/19-damage-failure.pdf>; 2005

Alvarado-Contreras J.A, Polak MA, Penlidis A, Constitutive modeling of damage evolution in semicrystalline polyethylene. J. Eng. Mater. Technol, 2010.132(4): 041009.

ASTM F1041-20, Standard Guide for Squeeze-Off of Polyolefin Gas Pressure Pipe and Tubing, ASTM International, West Conshohocken, PA, 2020.

*ASTM F 1734-19 Standard Practice for Qualification of a Combination of Squeeze Tool, Pipe, and Squeeze-Off Procedures to Avoid Long-Term Damage in Polyethylene (PE) Gas Pipe. ASTM International, West Conshohocken, PA, 201**9**.*

ASTM D732-17, Standard Test Method for Shear Strength of Plastics by Punch Tool, ASTM International, West Conshohocken, PA, 2017. < https://www.astm.org/Standards/D732.htm>

Ayoub G, Zaïri F, Naït-Abdelaziz M, Gloaguen J.M, Modelling large deformation behaviour under loading–unloading of semicrystalline polymers: application to a high density polyethylene, Int. J. Plast, 2010. 26: 329–347.

Azevedo C.R.F, Failure analysis of a crude oil pipeline, Eng. Fail. Anal. 14:978–994. <http://www.sciencedirect.com/science/article/pii/S135063070600210X>.

Barker M.B, Bowman J, Bevis M, the performance and causes of failure of polyethylene pipes subjected to constant and fluctuating internal pressure loadings, J. Mater. Sci. 18 (1983) 1095–1118. <http://link.springer.com/article/10.07/BF00551979>.

Betten J, Sklepus S, Zolochevsky A, A microcrack description of creep damage in crystalline solids with different behaviour in tension and compression, Int. J. Damage Mech. 8 (1999) 197–232. <http://ijd.sagepub.com/content/8/3/197>.

Bonora N, Gentile D, Pirondi A, and Newaz G, 2005, "Ductile Damage Evolution under Triaxial State of Stress: Theory and Experiments," International Journal of Plasticity, **21**(5), pp. 981–1007.

Brown N, and Crate J. M., 2012, "Analysis of a Failure in a Polyethylene Gas Pipe Caused by Squeeze off Resulting in an Explosion," J Fail. Anal. and Preven, **12**(1), pp. 30–36.

Brown N and Crate J.M, "Analysis of a Failure in a Polyethylene Gas Pipe Caused by Squeeze off Resulting in an Explosion," Fail. Anal. and Preven. J. Pennsylvania. USA, vol. 12, pp. 30–36, December 2011.

Brostow W, Corneliussen R.D. Failure of Plastics. Munich, New York: Hanser Pub; 1989. Cawood MJ, Channell AD, Capaccio G. Crack initiation and fibre creep in polyethylene. Polymer. 1993; 34(2): 423-425.

Celentano D. J., and Chaboche J.-L, 2007, "Experimental and Numerical Characterization of Damage Evolution in Steels," International Journal of Plasticity, **23**(10–11), pp. 1739–1762.

Chudnovsky A, Zhou Z, Zhang H., and Sehanobish K, 2012, "Lifetime Assessment of Engineering Thermoplastics," International Journal of Engineering Science, **59**, pp. 108–139.

Cheng J, Polak M, Penlidis A. A tensile strain hardening test indicator of environmental stress cracking resistance. J Macromol Sci Pure and Applied Chemistry. 2009; 45(8): 599-611. <https://www.tandfonline.com/doi/abs/10.1080/10601320802168728>.

Detrez F, Cantournet S, Seguela R, Plasticity/damage coupling in semicrystalline polymers prior to yielding: micromechanisms and damage law identification, Polymer, 2011, 52 :1998–2008. <http://www.sciencedirect.com/science/article/pii/S0032386111002023>.

Dhouibi S, Boujelbene M, Kharrat M, Dammak M, Maalej A, Friction Behavior of High-Density Polyethylene (HDPE) Against 304L Steel: An Experimental Investigation of the Effects of Sliding Direction, Sliding History and Sliding Speed, Journal of Surfaces and Interfaces of Materials, 2013; 1(1): 71–76. < https://www.ingentaconnect.com/content/asp/jsim>

Drozdov A.D, Christiansen J.d, Creep failure of polypropylene: experiments and constitutive modeling, Int. J. Fract. 159 (2009) 63–79. <http://link.springer.com/article/10.1007/s10704-009-9384-x>.

Dufailly J, Lemaitre J, Modeling very low cycle fatigue, Int. J. Damage Mech, 1995, 4:153–170. <http://ijd.sagepub.com/content/4/2/>.

Egugen A and Emilia O.M, "Determining the Forces in the Polyethylen Pipes after Squeeezing Them off with Specific Equipments," AEECE, 2015 [International Conference on Advances in Energy, Environment and Chemical Engineering].

Fleissner M, Experience with a full notch creep test in determining the stress crack performance of polyethylenes, Polym. Eng. Sci. 38 (1998) 330–340,

Frank G.J, Brockman R.A, A viscoelastic–viscoplastic constitutive model for glassy polymers, Int. J. Solids Struct, 2001. 38: 5149–5164.

Gu G, Xia Y, Lin C.-h, Lin S, Meng Y, and Zhou Q, Experimental study on characterizing damage behavior of thermoplastics, Mater. Des. 44 (2013) 199–207.

Harris K.E, "Squeeze-off& gel patch repair methods for polyethylene pipe in natural gas distribution lines", Corvallis.USA: Organ State University, 2007.

Hasan F, Iqbal J, Ahmed F, Stress corrosion failure of high-pressure gas pipeline, Eng. Fail. Anal. 14 (2007) 801–809.

Hernández-Rodríguez M.A.L, Martínez-Delgado D, González R, Pérez Unzueta A, Mercado-Solís R.D, Rodríguez J, Corrosive wear failure analysis in a natural gas pipeline, Wear 263 (2007) 567–571. <http://www.sciencedirect.com/science/article/pii/S0043164807004590>.

Hong K, Rastogi A, Strobl G, A model treating tensile deformation of semi crystalline polymers: quasi-static stress_strain relationship and viscous stress determined for a sample of polyethylene, Macromolecules, 2004, 37:10165–10173, http://dx.doi.org/10.1021/ma049174h.

Humbert S, Lame O, Chenal J.M, Rochas C, Vigier G, New insight on initiation of cavitation in semicrystalline polymers: in-situ SAXS measurements, Macromolecules, 2010, 43:7212–7221.

Hyde T.H, Sun W, Williams J.A, Life estimation of pressurised pipe bends using steady-state creep reference rupture stresses, Int. J. Press. Vessels Piping, 2002, 79: 799–805.

ISO 16770, 2004, "Plastics-Determination of Environmental Stress Cracking (ESC) on Polyethylene (PE) – Full Notch Creep Test (FNCT)."

ISO 16241, 2005, Notch Tensile Test to Measure the Resistance to Slow Crack Growth of Polyethylene Materials for Pipe and Fitting Products (PENT), International Organization for Standardization.

ISO 9080, Plastics Piping and Ducting Systems-Determination of the Long-Term Hydrostatic Strength of Thermoplastics Materials in Pipe Form by Extrapolation, International Organization for Standardization, 2012.

ISO 16770, Plastics-Determination of Environmental Stress Cracking (ESC) on Polyethylene (PE) – Full Notch Creep Test (FNCT), International Organization for Standardization, 2004.

Jar P.Y.B, A New Concept of using Transverse Loading to Characterize Environmental Stress Cracking Resistance (ESCR) of Polyethylene (PE), Res Dev Material Sci, 3(5), 2018.

Jar P.-Y. B, "Effect of Tensile Loading History on Mechanical Properties for Polyethylene," Polym Eng Sci, **55**(9), pp. 2002–2010, 2014.

Jar P.-Y. Ben, Muhammad S, "Cavitation-induced rupture in high-density polyethylene copolymers", Polymer Engineering & Science. J vol. 52, pp. 1005–1014, November 2011.

Jar B, Ward P, Jar Ch, Zhang Y. A New Method to Characterize Environmental Stress Cracking Resistance (ESCR) of Polyethylene (PE) and its Pipes, in: ANTE 2017 The Plastic Technology Conference, Anaheim California, 2017.

Kiass N, Khelif R, Boulanouar L, and Chaoui K, 2005, "Experimental Approach to Mechanical Property Variability through a High-Density Polyethylene Gas Pipe Wall," J. Appl. Polym. Sci., **97**(1), pp. 272–281.

Kramer E.J, Environmental cracking of polymers, in "Developments in Polymer Fracture. Vol. 1. Andrews EH (ed), Applied Science, London, Chap. 3 (1979).

Kramer. EJ. Developments in polymer fracture. London, England: Applied Science Publishers; 1979.

Krishnaswamy R.K, 2005, "Analysis of Ductile and Brittle Failures from Creep Rupture Testing of High-Density Polyethylene (HDPE) Pipes," Polymer, **46**(25), pp. 11664–11672.

Kurelec L, Teeuwen M, Schoffeleers H, and Deblieck R, 2005, "Strain Hardening Modulus as a Measure of Environmental Stress Crack Resistance of High-Density Polyethylene," Polymer, **46**(17), pp. 6369–6379.

Kwon I.H.J, P.-Y. Jar Ben. On the application of FEM to deformation of high-density polyethylene. International Journal of Solids and Structures, 2008,45(11-12):3521-3543**.**

Lemaitre J, and Dufailly J, 1987, "Damage Measurements," Engineering Fracture Mechanics, **28**(5–6), pp. 643–661.

Lustiger A, Understanding environmental stress cracking in polyethylene. In: Portnoy RC, editor. Medical plastics: degradation, resistance & failure analysis, Medical Plastics, 1998, p. 66-71.

Lang R.W, Stern A, Doerner G, Applicability and limitations of current lifetime prediction models for thermoplastics pipes under internal pressure, Die Angew. Makromol. Chem. 247 (1997) 131–145.

Majid Z.A., Mohsin R, Yaacob Z, and Hassan Z, 2010, “Failure Analysis of Natural Gas Pipes,” Engineering Failure Analysis, **17**(4), pp. 818–837.

Muhammad S, Jar P.-Y.B, Determining stress–strain relationship for necking in polymers based on macro deformation behavior, Finite Elements in Analysis and Design.J, vol. 70–71, pp. 36–43, September 2013

Muhammad S, Jar P.Y.B, Effect of aspect ratio on large deformation and necking of polyethylene, J. Mater. Sci. 2011, 46, 1110–1123.

Muhammad S, Jar P.-Y.B. Determining stress–strain relationship for necking in polymers based on macro deformation behavior, Finite Elements in Analysis and Design. J, 2013, 70–71: 36–43.

Palermo G, “ Correlating Aldyl “A” and Century PE Pipe Rate Process Method Projections with Actual Field Performance”, 2004, Milan. Italy.[Plastics Pipes XII Conference].

“PE Squeeze-Off Tools - Reed Manufacturing” [Online]. Available: https://www.reedmfgco.com/en/products/plastic-pipe-tools/pe-squeeze-off-tools/. [Accessed: 09-Feb-2017].

Pinter G, Haager M, Balika W, and Lang R.W, 2007, “Cyclic Crack Growth Tests with CRB Specimens for the Evaluation of the Long-Term Performance of PE Pipe Grades,” Polymer Testing, **26**(2), pp. 180–188. [10] Palermo, G., 2004, “Correlating Aldyl ‘A’ and Century PE Pipe Rate Process Method Projections with Actual Field Performance,” *Plastics Pipes XII Conference. Milan, Italy*.

Rose LJ, Channell AD, Frye CJ, Capaccio G. Slow crack growth in polyethylene: a novel predictive model based on the creep of craze fibrils. J Appl Polym Sci.1994; 54(13): 2119-2124.

Rouse J.P, Sun W, Hyde T.H, Morris A, Comparative assessment of several creep damage models for use in life prediction, Int. J. Press. Vessels Piping, 2013, 108–109 :81–87.

Schneider K, Trabelsi S, Zafeiropoulos N.e, Davies R, Riekel C, Stamm M, The study of cavitation in HDPE using time resolved synchrotron X-ray scattering during tensile deformation, Macromol. Sympos,2006. 236:241–248.

Scheirs J. Compositional and failure analysis of polymers: A practical approach, Wiley, Chichester; 2000, p.556-561.

Shalaby H.M, Riad W.T, Alhazza A.A, Behbehani M.H, Failure analysis of fuel supply pipeline, Eng. Fail. Anal. 13 (2006) 789–796.

Stephens D.R, Cassady M.J, Leis B.N, “Progress report on preliminary screening tests on squeeze-off of polyethylene gas pipes”, Battelle, Columbus, OH (United States), January 1987-December 1989.

Stephens D.R., Leis B.N, Francini R.B, Cassady M.J, “Users’ guide on squeeze-off of polyethylene gas pipes”, vol.1, August 1989-February 1992. Battelle, Columbus, OH (United States).

U.S. Department of Transportation, 2017. PHMSA - Data & Statistics [WWW Document]. US Department of Transportation.

Uzelac D, Bikiae S, Durdeviae M, Bordeasu I, “Change of Polyethylene Pipe Wall Thickness after Squeezing Using Squeeze off-Tool”, Materiale Plastice .J, vol.47, pp.461–466, December 2010.

Viana J.C., Structural interpretation of the strain-rate, temperature and morphology dependence of the yield stress of injection molded semicrystalline polymers, Polymer 46 (2005) 11773–11785.

Wright D. C, Environmental stress cracking of plastics. Smithers Rapra Technology Ltd., Shawbury, UK (1996).

Yayla P, Bilgin Y, “Squeeze-off of polyethylene pressure pipes: Experimental analysis”, Polymer Testing. J, vol. 26, pp.132–141, 2007.

Zhang Y, Jar P.-Y, “Effect of squeeze-off on mechanical properties of polyethylene pipes”. International Journal of Solids and Structures.J, vol. 135, pp. 61–73, November 2017.

Zhang Y, Jar P.Y. Ben, Phenomenological modelling of tensile fracture in PE pipe by considering damage evolution, Materials and Design, 77 (2015) 72-82.